Ca' Foscari
University
of Venice

Master's Degree programme

in Conservation Science and Technology

for Cultural Heritage

Final Thesis

A significant contribution to the conservation of UNESCO sites in Armenia. Study of the state of conservation of the Geghard Monastery

Supervisor
Ch. Prof. Elisabetta Zendri

Graduand
Matilde Veneziano
Matriculation number 892168

Accademic Year
2022-2023

Index

Abstract

The preservation and conservation of built Cultural Heritage is a complex matter that needs to be monitored to develop appropriate monitoring and preventive conservation actions. In the Armenian context, this is something that is even more challenging, since most of the architectural heritages are monasteries not always easy to reach, and are also subjected to problems that go from geological and seismic hazards, to degradation of the architectural materials due to weathering.

This study consisted in the monitoring and preliminary analyses of the state of conservation of Geghard Monastery, one of the most important UNESCO heritage sites in Armenia. Specifically, this research reports the preliminary results of the multi-disciplinary investigation on the internal stone surfaces of the caved rooms of the Geghard complex: the "Proshian family room" (*Žamatoun*) belonging to the XIII century [1].

Non-destructive and easy-to-use analyses were performed to evaluate the current situation and suggest a possible monitoring plan. A photographic survey and morphological analysis of the stone surfaces were carried out to precisely map the degradation patterns. The monitoring of temperature and humidity was also measured by a datalogger located in the *Žamatoun*. Sponge-test method [2] was applied at different heights and positions in the room to evaluate the stone's behaviour with water. Ultrasonic analyses were also conducted to collect information on the weathering of different areas in the chamber. Together with these measurements, chemical and mineralogical analyses on the widespread presence of black deposits and efflorescence were performed in the lab by FTIR, Raman, salt conductivity, and XRD analyses to try to understand their formation processes.

The collected data constitute a starting point for understanding the state of conservation of the caved room, helpful for future preventive conservative interventions.

Keywords: Armenia, Geghard monastery, Ultrasonic measurements, FTIR, Sponge-test method

<u>Aim of the thesis work</u>

This thesis work presents the diagnostic campaign conducted in situ and in the laboratory on the cultural heritage site of Geghard monastery. Most of the work was carried out in situ thanks to the collaboration with the National University of Architecture and Construction of Armenia (NUACA) with the aim to give non-invasive methodologies guidelines and results useful for future monitoring and conservative interventions.

The non-invasive studies include a careful visual survey that consisted of the evolution assessment over 5 years and the development of a degradation map of the analysed room. These studies consisted also of the evaluation of the surface behaviour in the presence of water and the relative humidity of the first surface layers. Finally, ultrasonic analyses were also performed to examine potential internal problems. Every measurement was associated with a colour map to facilitate reading even for an untrained eye.

The humidity and temperature of the room under analysis were constantly monitored to also understand their possible relationships with the degradation phenomena. When possible, some samples were taken trying to be as less invasive as possible. This sampling campaign was fundamental for the laboratory analyses conducted such as FTIR, Raman, XRD, microscopic observations and measurement of soluble salts useful to deny or support the hypothesis that came up during the in situ investigation.

1. Introduction

Historic buildings are considered valuable architectural heritages that define the cultural and historical context of each place. According to ICOMOS [3] "The value of architectural heritage is not only in its appearance but also in the integrity of all its components as a unique product of the specific building technology of its time". It is thus clear the importance of preserving this legacy that unfortunately often comes up against many conservative problems due to both natural and human actions. There are many examples around the world of this kind of heritage that can be found both in an urban environment or in more secluded places surrounded by nature. These last cases, most of the time consist of temples, fortresses, or monasteries like the Geghard monastery (Armenia) which, due to their immovable structures, could result in a challenge for their conservation and maintenance. The problems that we can face with these kinds of structures are mostly the same as buildings in urban areas: geological hazards (earthquakes, subsidence, floods etc.) and microclimate problems that frequently lead to the

weathering of the object. However, the not-so-easy access to these kinds of architectural heritages can augment the challenge of conservation. A prompt intervention could be something not feasible compared to the ones in an urban context. Another problem could be the instrument and investigations to conduct during a conservation campaign. Portable instruments sometimes could be difficult to carry around and require a good wireless system and a long-life battery. For these reasons a more accurate management and organization program is essential.

Additionally, historic buildings can face a great variability of materials and architecture together with their transformations over time. For this, is important to always distinguish case by case and apply the most feasible analytical approach for the survey considering all the context variables. Often happened, indeed, that inappropriate previous interventions have worsened the original situation of the heritage highlighting the importance and necessity of studies and monitoring. The multidisciplinary approach is also something that should be engaged whenever possible [4]. The intervention of different experts in other fields could really lead to applying the most accurate approach according to the degradation phenomena present, the history of the monument as well as its previous restoration interventions, the rock typology, the architectural structure etc.

Preliminary analyses in the cultural heritage field are essential for thoroughly comprehending the heritage situation, aiding in understanding its development over time and its protection and prevention. These analyses that should always carried out, establish the fundamental groundwork upon which conservation and restoration works should be constructed, thereby guaranteeing the preservation of the cultural heritage.

1.2. The Geghard Monastery

The Geghard monastery (Fig. 1) is one of the three cultural heritages of Armenia registered in the UNESCO Heritage list. This, along with its proximity to the capital Yerevan (42 Km), the particular architecture largely carved into the rock and the fact that still is a consecrated church, makes it one of the most visited monasteries in the territory. However, despite the importance of this monastic complex, diagnostic studies for its conservation are practically absent. For this reason, the preliminary investigations carried out for this thesis work result to be of fundamental importance.

Figure 1. The monastic complex of Geghard.

1.2.1 History and description

The monastery has a troubled history that dates back to 300-400 believed to be the period of its first foundation in accordance with the oral tradition and the XIII century historian Vardan Patmitch [5]. Over the years, many construction and later restoration works have been evidenced by some inscriptions, but the descriptions of past works are unluckily not well documented.

The existing complex of Geghard was built in the first quarter of the XII century and consists of a main church "*Kathoghikè*", a "*gavit*" (Entrance Hall), two churches carved inside the rock and two "*Žamatoun*" (Gavit-cementary) [1]. Many rock chapels and cells can also be found within the monastery walls as well as in the surrounding mountains.

The *Kathoghikè* was built in 1215 during the Zakarian reign and its architecture is typical of the Armenian period between the XII and XIII centuries: a cross-shaped plan inscribed in a square and then covered by a dome [1]. The main church's *Gavit* is delineated by 4 massive columns that separate the squared space where in the centre a dome with stalactites is observable. The two stone churches are located then in the north side of the monastery. One of these is known for the presence of a natural spring which crosses the room, and the other is the one adjacent to the *Žamatoun,* main object of this study. This latter is known also as the "Proshian family chamber" due to their sculpted emblem: two lions siding an ox's head and an eagle holding a sheep in its claws. This room is also characterized by a variety of decorative and iconographic themes all over the walls. The upper *Žamatoun* instead dates to 1288, under

the reign of Papak (the son of Prince Prosh) and his wife Rousakan [1]. Here again, 4 central columns within a square-based area can be observed.

1.2.2. Geological and environmental context

The geology of Armenia is characterized by a vast variety of landscapes which change from region to region strictly related to volcanism, particularly relevant tectonic processes for the last 250 million years, and the three main crustal fragments: the South Armenian Block, the Sevan-Akera and the Eurasian Block (Fig. 2b). The movement between the Eurasian and Arabian Plates is one of the main causes why the territory is subjected to earthquakes. These are also related to the stratovolcanoes, known for their periodic violent explosive eruptions that often end with destructive seism. Some of the oldest earthquakes were documented in 893 and 906 destroying the city of Dvin. Even the capital Yerevan was subjected to quakes several times, in particular, the 1679 event (8-9 degrees on the Mercalli scale) near Garni struck most of the surrounding territory, including the Geghard monastery [6,7].
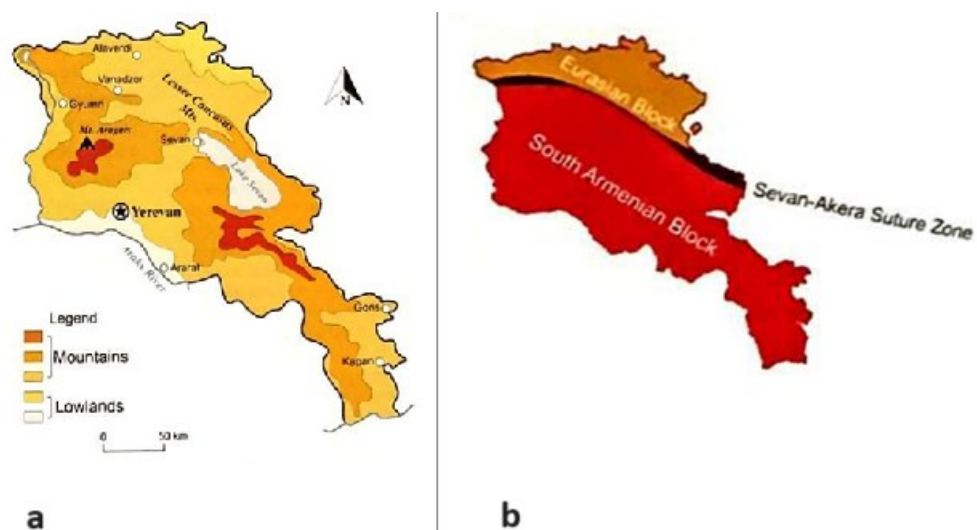

Figure 2. Semplified geological maps of armenia. a) semplified map depicting the distribution of lowlands and highlands; b) Small map of Armenia showing the two major tectonic blocks with the main Sevan-Akera Suture Zone (Siegesmund, Gross, Oriolo, & Lorsabyan, 2022).

Armenia is featured mostly by mountains (Fig. 2a) and has a continental climate characterized by cold winters and hot summers reaching values from -10 °C up to 45 °C [8]. Geghard monastery is in the Kotayk region and rises at 1750 m above sea level. This region has been subjected to large-scale fissure eruptions that lead to large basaltic lava flows creating also the characteristic hexagonal stones also observable in the near province of Garni (7 km away from Geghard) [7]. The Geghard strata group of volcanic origin is marked by yellowish and grey tuff alternated with brecciated datolite tuff and the surrounding stones are believed to be formed

between 7-12 million years ago [6]. The monastery is surrounded by fascinating mountains and vegetation.

1.2.3. Materials and state of conservation from literature

According to Siegesmund et al. [9] and Wedekind et al. [10] the main stones present in Geghard are identified as tuff and basalt both divisible in two different typologies. The tuff is divided in accordance with its clast content:

- Fine-grained tuff (almost free of clastic material) shows a high porosity of 38 vol %, moderate water uptake of $\pm$ 5 kg/m^2/h and a hydric expansion of 0,5 mm/m.

- High proportion of clasts tuff shows lower porosity (30 vol %) but double the capillarity water uptake ($\pm$ 12 kg/m^2/h) and hydric expansion (1,0 mm/m).

Basalt can be differentiated into:

- Homogenously porous basalt (23,5 vol %).

- Laminated, much harder variety with isolated macropores and lower porosity (17,4 vol %).

During the first International Summer School "Stones in Armenian Architecture" in 2019, damage investigations were carried out on two walls of the monastery: the external east wall and the west wall of the Proshian family room. Figure 3 reports the two degradation maps resulting from this study. In either case, the presence of salts (sulphates and nitrates) and cracks associated with the seismic activities are highlighted. According to their observations also hydric expansion and sanding are present as main degradation patterns. Wedekind et al. [10] also conducted some ultrasonic analyses to try to understand the behaviour of the two typologies of tuff according to their composition and content of water observing that ultrasound velocity decreases in both rock varieties in water-saturated conditions.
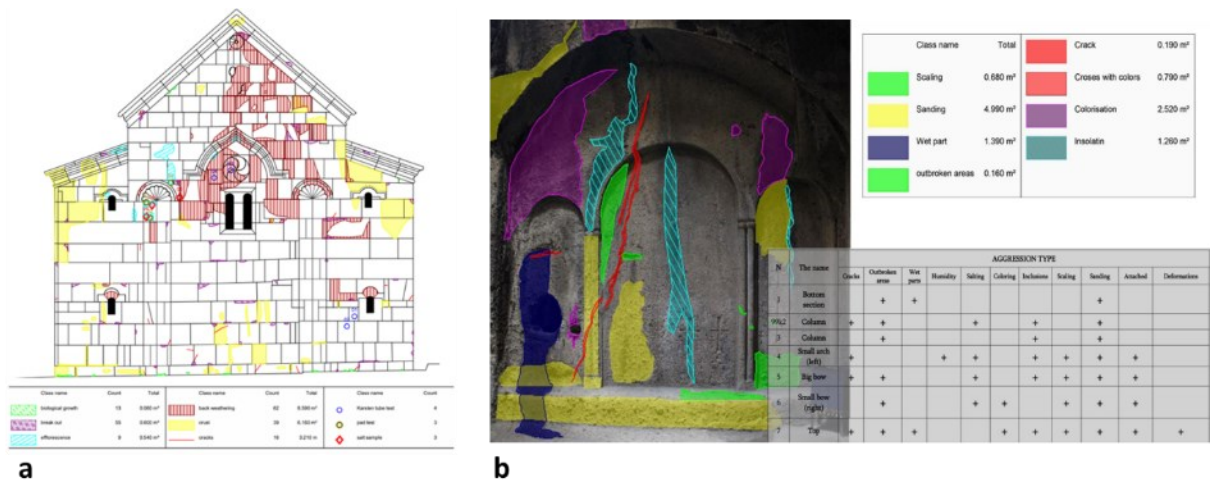
Figure 3. Figure 3. Degradation maps resulted from the 2019 investigations. a) degradation map of the external eastern wall (Wedekind, Harutyunyan, Novaković, & Siegesmund, 2020); b) degradation map of the western wall of the Proshian family room (PowerPoint presentation – results of the first summer school "Stones in Armenian Architecture", 2019).

1.2.4. The Proshian family room

The Proshian family room is the area where most of the investigations conducted during this thesis work were done (Fig. 4). This choice is linked to the analyses that were already carried out in 2019 during the summer school organized by the National University of Architecture and Construction of Armenia (NUACA), and the willingness to compare what was found in the past and eventually upgrade it. In 2019 indeed a damage assessment of the western wall of the *Žamatoun* was carried out resulting in a degradation map. This last, even though does not follow the standardized ICOMOS glossary, could be useful anyway to understand how the situation has changed over the years. For this reason, the research area is taken under consideration in the most recent analysis.
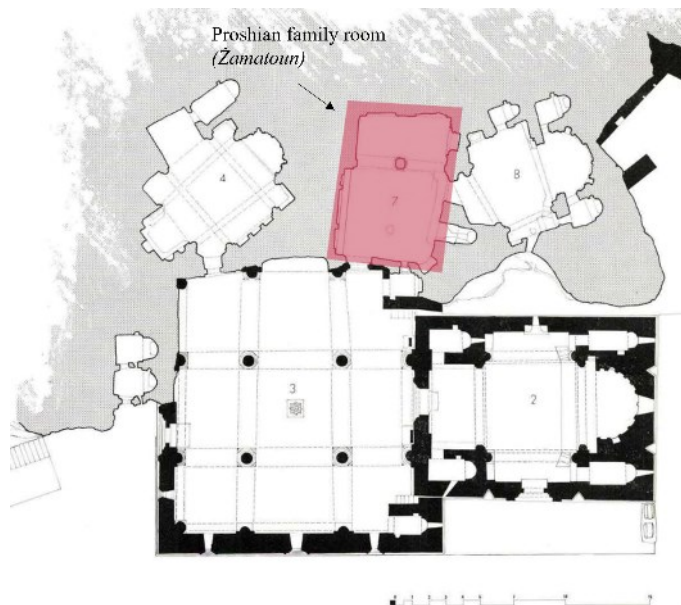

Figure 4. First floor planimetry of Geghard Monastery, highlighted the Proshian familiy room (Žamatoun) (by Ara Stepanian, Telman Gevorgian, Edik Hovhannisian, Hratchia Gasparian & Edward Frangoulian, 1971).

1.2.5. Restoration works record

Due to the high seismic activity to which Armenia is subjected, Geghard monastery was restored a lot of times with also the total reconstruction of some parts; indeed to this day, nothing has remained of the original monastic complex [11]. According to Vahramian [5], the inscriptions that testify the restoration works done start from 1257-1258. In 1655 according to some evidence, Soulé son of Tgha of the city of Tbilisi, financed a series of restoration works in the monastery; during this occasion, the dome of the main church was completely redone. Then, in 1696 after the damages caused by the Garni earthquake of 1679, the reconstruction and restoration of the monastery began. There is also evidence of restoration works in 1708 followed by those carried out between 1969-1972 which consist of the enlargement of the courtyard, demolition and replacement of the two-floor building containing the monk's cells with a one-floor building; numerous *Khatchkar* (engraved Armenian cross on stele) were discovered and inserted on the walls of the secondary *ex-novo* constructions of the monastery.

In accordance with Mery Danielyan, one of the restores that worked in Geghard [12], in the last fifty years, large-scale restoration works were carried out comprehending the closing of cracks present in the carved rock structure. In 1978 drainage studies were carried out and a tunnel was built to divert into the river the rainwater and the water from the spring located in the near surrounding and passing through the monastery. Despite the drainage system was cleaned recently in 2021, according to Danielyan the network is in decay. The closing of the cracks happened in more than one step, at first it was used a polymerized non-solidifying and self-adhesive "tape"[i], but it did not reach the hoped results. For this reason, in 2015 it was started to be used a thixotropic mortar to seal the cracks after washing them through high-pressure water. The mortar used was probably the "Mapegrout T40" as suggested by Arzumanyan et al. [13].

In 1990s the roof of the *Kathoghikè* and the *gavit* was restored with the use of metal coverings that were then replaced in 2017 with basalt tiles. In this year, a restoration and renovation plan was conducted during which new basalt plates were used to fill missing sections on the floor and in the ceiling. Also, lime mortar was applied in all types of fillings. Before the use of this mortar, sand, cement and gravel were also used.

In future interventions, Mery Danielyan also proposes to plaster from the inside of the walls and arches with mortar and on the surfaces to use waterproof paint. She also proposed to cover the walls on the outside with large semi-finished basalt stones; for the interior portion of the

---

[i] There are some uncertainties about this term used correlated to a possible mistake during the translation between Armenian and English.

wall she suggests to pack it with chips and lime mortar claiming that the stones should be wetted to avoid mortar moisture from being extracted.

A lot of these restorations over the years consisted of the demolition and reconstruction of the original structures. This tendency is probably linked to the fact that this church is still consecrated and, to continue its use, they consider more important its functionality rather than its heritage value. This was also noticed when in May 2023 – period of the in situ investigations reported in this thesis – some works were carried out on the external pavement that consisted of a mortar laying to make people reach the church in an easier way.

[1] Sahinian A. Il complesso monastico di G(h)eghard. In: Documenti di Architettura Armena | G(h)eghard. Edizioni Ares; 1973

[2] UNI Normal 11432-2011, Beni culturali, Materiali lapidei naturali ed artificiali - Misura della capacità di assorbimento di acqua mediante spugna di contatto

[3] icomos.org (Internet). ICOMOS charter Principles for the analysis, conservation and Structural Restoration of Architectural Heritage, ICOMOS international council on monuments and sites. 2003 (accessed on: September 2023). Available at: https://www.icomos.org/en/about-the-centre/179-articles-en-francais/ressources/charters-and-standards/165-icomos-charter-principles-for-the-analysis-conservation-and-structural-restoration-of-architectural-heritage

[4] Valluzzi M. R. On the vulnerability of historical masonry structures: analysis and mitigation. In: Materials and Structures. RILEM; 2006

[5] Vahramian H. Breve cronologia storica. In: Documenti di Architettura Armena | G(h)eghard. Edizioni Ares; 1973

[6] Aslanian A. La struttura geologica della zona di G(h)eghard. In: Documenti di Architettura Armena | G(h)eghard. Edizioni Ares; 1973

[7] Siegesmund S., Gross C. J., Oriolo S., Lorsabyan T. THE ARMENIAN GEOLOGICAL RECORD Drifting Continents, Earthquakes, Volcanism, Landscapes and Geological Resources. In: Armenien. Kultur Natur Menschen. Mitteldeutscher Verlag; 2022

[8] Ruggieri R., Davtyan S., Shaihinyan S., Ugujyan A., Orsini R., et al. Armenian karst project. In: Carbonates and Evaporites. Springer; 2022

[9] Siegesmund S., Pötzl C. BUILDING STONES OF ARMENIA Conservation and restoration measures as resource protection. In: Armenien. Kultur Natur Menschen. Mitteldeutscher Verlag; 2022

[10] Wedekind W., Harutyunyan E., Novaković N., Siegesmund S. Experimental Conservation and first Investigations on the Weathering of Geghard Monastery (Armenia). In: Monument Future: Decay and Conservation of Stone – Proceedings of the 14th International Congress on the Deterioration and Conservation of Stone. Mitteldeutscher Verlag; 2020

[11] Koppel T., Haldre H. Ground electrostatic field indicating subsurface water measurements in Geghard monastery, Armenia. In: Proceedings of "Earth's fields" conference; 2018

[12] Danielyan M. RESTORATION OF HISTORICAL AND ARCHITECTURAL MONUMENTS IN ARMENIA Reconstruction and restoration of Geghardavank. In: Armenien. Kultur Natur Menschen. Mitteldeutscher Verlag; 2022

[13] Arzumanyan A. A., Arzumanyan A. A., Qaramyan H. H., Muradyan N. G. CONCEPTUAL APPROACHES TO SOLVING THE ISSUE OF REINFORCING THE ROCK - CUT STRUCTURES OF GEGHARD MONASTERY COMPLEX. In: Architectural and Engineering Research; 2021

2. Materials and Methods

This chapter is divided into two main sections according to the analysis carried out in situ and in the laboratory.

In situ analyses

The advantages of in situ measurements are not to be ignored since they allow us to know the general situation of the object under analysis. Moreover, if we consider specially built heritage, it must be specified that micro-analyses on some specific point may not be representative. Portable instruments in this sense play an important role in a better understanding of the object as a whole [14]. Moreover, these surveys are of great importance in the selection of micro-samples for laboratory analyses [15].

In the following Figure (Fig. 5), is reported a brief description of what we would like to know or get associated with the conducted investigation used.
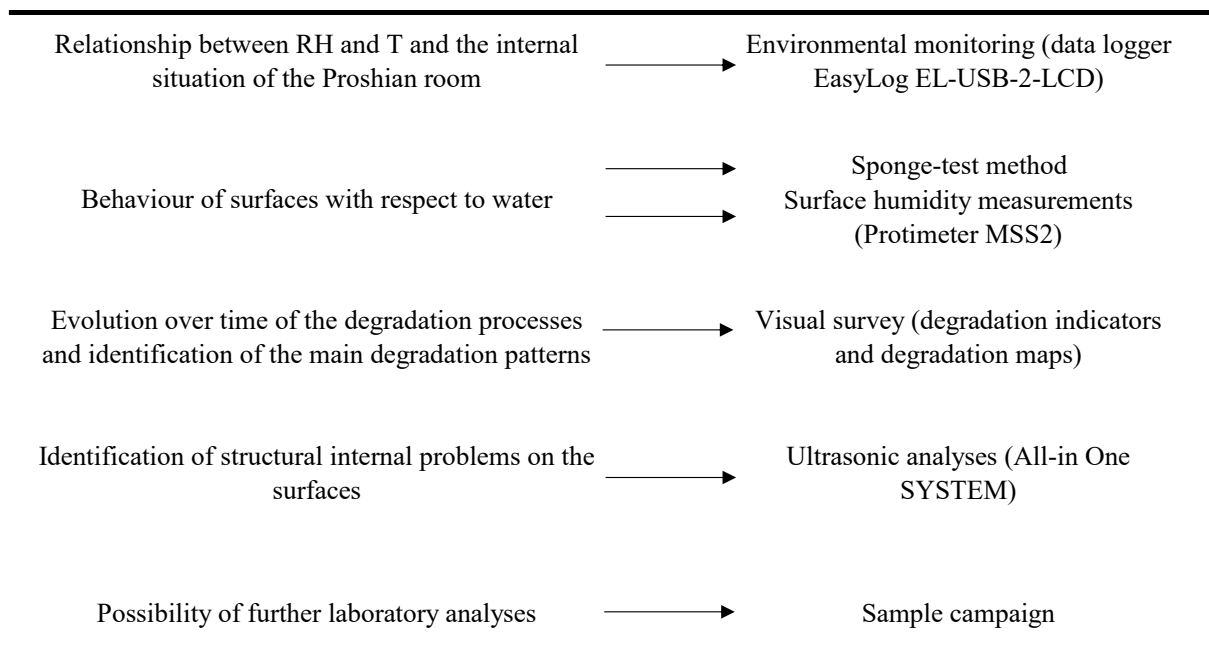
Relationship between RH and T and the internal situation of the Proshian room	→ Environmental monitoring (data logger EasyLog EL-USB-2-LCD)
Behaviour of surfaces with respect to water	→ Sponge-test method → Surface humidity measurements (Protimeter MSS2)
Evolution over time of the degradation processes and identification of the main degradation patterns	→ Visual survey (degradation indicators and degradation maps)
Identification of structural internal problems on the surfaces	→ Ultrasonic analyses (All-in One SYSTEM)
Possibility of further laboratory analyses	→ Sample campaign

Figure 5. Summary scheme of in situ analyses conducted along with their purpose.

2.1. Environmental monitoring

The environmental conditions were monitored with a datalogger *EasyLog EL-USB-2-LCD* which allows the measurement of air humidity and temperature at arbitrarily decided periods. For this case study, the instrument was located at a height of ± 3 m on the architrave of the

entrance of the analysed room from 25/04/2023 until 02/06/2023. Temperature and humidity were measured every 30 minutes.

According to Camuffo [16] the use of this instrument sited in a corner of a room, even though very common, is not properly accurate. Dataloggers furnish representative data only of the point where the sensor is located, not of the whole room. For this reason, the best solution should be the possibility to put the same instrument in different areas of the room along a chosen regular grid.

Additionally, to have more appropriate and representative results that can be compared with the room under analysis, the ideal would be to have the measurements for an entire year. This allows us to have a good general idea of the temperature fluctuations that could be related in some ways to the internal degradation processes that are going on. However, all these requirements and suggestions cannot always be applied, as in the case of the Geghard Monastery where the lack of appropriate surveillance, does not permit keeping the instrument wherever necessary. In fact, initially, there was another datalogger placed at ± 1,5 m but that disappeared after a few days causing the impossibility of having more precise results (Fig. 6).

Figure 6. Localization of the dataloggers. a) first datalogger position; b) second and lost datalogger position.

2.2. Visual survey: degradation map and degradation indicators

A visual survey is the first step to pursue, once a research and/or conservation campaign on cultural heritage monuments has been planned. The importance of visual surveys relies on having a general idea of the current situation under analysis. Thus, these surveys are essential to have a clearer understanding of the state of conservation of the monument and the main degradation phenomena with their extension and possible causes.

These evaluations should always be paired with photographic documentation, which was done also in the Geghard complex, paying more attention to the Proshian family room, where also degradation maps of the different sections of the space were constructed following the ICOMOS glossary guidelines [17]. This latter, according to the then ICOMOS President Prof. Dr. Michael Petze "constitutes an important tool for scientific discussions on decay phenomena and processes" [17].

The degradation maps were made using the *AutoCAD* drawings shared by Arch. Nanar Kalantarian and subsequently modified according to the needs, and *GIMP-Image manipulation program* to highlight the different degradation patterns. These maps are fundamental to have an immediate view of the situation and it is necessary that are understandable by everyone so that they can be a base for future interventions and analyses. To complete this survey in the room, microscopic pictures were also taken in visible and UV light with a Dino-Lite portable microscope (magnification: 51,3x; unit: mm).

In the rest of the complex, the focus was more on the presence of structural problems (i.e., fractures) and differences with the situation in the past. With this aim, 9 pictures have been compared to others that date back to 2018 and kindly given by Dr Ing. Daniele Spizzichino (ISPRA). The comparison was useful in understanding the development of the situation over five years. According to these, a table based on the concept of the damage categories that Fitzner et al. [18] suggested, has been constructed. Differently from them, it was decided to consider the overall situation that is visible from the pictures and not the single degradation pattern. However, notwithstanding the fact that for this reason, it was decided to use the term "degradation indicators" and not properly the term "damage categories", we still applied the same scale used by Fitzner et al. (0 – no visible damages; 5 – very severe damages). The decision to evaluate a more critical situation is based on the presence and quantity of fractures as well as the quantity and presence of salt encrustations. Where possible, the change of colour of a certain area – not associated with different light exposition – is also evaluated.

Fitzner et al. also defined the linear damage index corresponding to the average damage category, and the progressive damage index which emphasizes the proportion of higher damage categories. Both these indices are calculated following Equation 1a, b.

Equation 1. Formulas of (a)"Linear damage index", (b) "Progressive damage index".

(a)
$$DI_{lin} = \frac{B + (C \cdot 2) + (D \cdot 3) + (E \cdot 4) + (F \cdot 5)}{100}$$

(b)
$$DI_{prog} = \sqrt{\frac{B + (C \cdot 4) + (D \cdot 9) + (E \cdot 16) + (F \cdot 25)}{100}}$$

B = damage category 1; C= damage category 2; D= damage category 3; E damage category 4; F= damage category 5.

In this thesis work, the linear and progressive damage indices were also calculated according to the formulas above (Eq. 1a, b) considering the overall situation visible from the selected pictures from 2018 and 2023, thus, the degradation indicators were used in place of the damage categories.

2.3. Surface humidity

It is well-known that the presence of water inside a stone material can be one of the main causes of deterioration [19,20]. For this reason, the monitoring of surface humidity turns out to be important to assess the state of conservation of the monument: knowing the distribution of moisture inside the material can help us understand the possible cause of the water's presence and how to remove it or reduce it.

In the Proshian family room, the instrument used for a semi-quantitative distribution of the water is the *Protimeter MMS2* provided by NUACA University with the "Pinless Moisture Meter" mode (Fig. 7). This instrument gives RH measurements ranging from 60-999 according to which the material is considered:

- dry (values between 60 and 170)

- at risk (values between 170 and 200)

- wet (values bigger than 200)

However, the instrument displays the surface moisture in terms of "Wood Moisture Equivalent" count and reliable readings are obtained only if the sensor bulge is in direct contact with the surface: conditions that in Geghard are frequently not satisfied because of the high heterogeneity of the surfaces. The instrument can nominally measure the water content until 19 mm in dense, homogeneous materials. The choice of using this specific instrument was dictated by the willingness to try to compare previous results taken during a 2019 summer school organized by NUACA University and the Georg-August-Universität Göttingen [10].

The analyses were made on all the vertical surfaces of the room in conformity to its morphology, the operator's height, and the extension of the arm reaching between 1,50 m and 1,80 m. The surface was thus divided into sectors where each measurement was spaced by $\pm$ 20 cm in length and 20/30 cm in height according also to the different matter, degradation process and architectural element. In the case of the octagonal column, this was considered as a single element, and it was tried to represent it with two drawings that show the 4 front faces visible from the centre of the room and the other 4 from the back of the column (under the vaulted zone). Here each measurement was taken at the centre of each face and at different heights spaced one by another of $\pm$ 20 cm. The results were then recorded on a colour map using *OriginPro* and the *AutoCAD* maps. Although this allows us to have an immediate view of the general distribution of the surface moisture, it must be considered that this instrument was probably not the best for the case study because of the impossibility of setting the different materials to be measured.

Figure 7. Application of Protimeter MMS2 in "Pinless Moisture Meter" mode.

2.4. Sponge test method

The sponge method [2] is a valid non-invasive way to measure the initial rate of water absorption that can give information about the behaviour of the first layers of the material under analysis [21]. This procedure is thus useful for understanding the properties of different materials.

In the case under analysis around 240 points were analysed always using the same kind of sponge (10 x 5,5 x 2 cm) with the same initial quantity of water and pressure applied per 30 seconds. The distance from one measurement to another was ± 40/50 cm, and the reached height hinged on the operator's extension of the arms. The measure consisted of soaking the sponge with water taken from the drinking fountains outside the church, squeezing away the excess water and weighing the sponge before and after the application of it on the selected point of the surface. The subtraction of these two weights corresponds to the water intake on the point measured.

For the measuring grid, it was tried to use the same of surface humidity measurements, but each point was spaced more one from another to have areas adequate for these measurements.

All the measured points were then reported in *g/cm² · sec* in a table according to the normative UNI Normal 11432-2011 equation (Eq. 2) [2], and on a coloured map – which helps to have a prompt view of the situation – the exact results of the subtraction.

Equation 2. Calculation of the water amount absorbed with the sponge-test method according to UNI Normal 11432-2011

$$WA \left(\frac{g}{cm^2} \cdot sec\right) = \frac{P_i - P_f - P_o}{S \cdot t}$$

P_i = initial weight in grams; P_f = final weight in grams; P_o = foreign object weight in grams (where necessary); S = contact surface of the sponge in cm²; t = contact time in seconds.

2.5. Ultrasonic analyses

The ultrasonic investigation is a non-destructive method to study the internal discontinuities of a material without affecting it. This method relies on analysing the wave velocity that crosses the selected object, enabling the assessment of intrinsic material properties, including homogeneity, the presence of fractures or cavities and the material strength. Thus, the results are based on the "travel time" or "time of flight" of the generated acoustic waves that cross the sample. Altered and weakened zones of the structures, along with the occurrence of

microfractures and material flaking, can be spotted by lower acoustic velocity values than in unaltered and intact materials [22].

The measurements can be performed with three different set-ups depending on the accessibility of the sampled stone:

- The *direct method*, where the two indicators (the source and the receiver) are on opposite faces of the analysed object.

- The *semi-indirect method*, where the indicators are placed at a given angle.

- The *indirect method*, where the indicators are on the same surface.

Knowing then the distances between the source (usually a piezoelectric transmitter that emits a frequency higher than 20 kHz) and receiver it is possible to calculate the wave velocity inside the material (Eq. 3). Usually, the time of flight of the analysed material is compared with its healthy counterpart or a reference standard [23]. Thanks to the comparison of these data, if the signal emitted by the transmitter arrives at a different time of flight to the receiver, it means that there could be some different features inside the analysed object. For instance, if the signal arrives later, it means that there are some discontinuities according to the characteristics of the stone. For this reason, ultrasonic data interpretation is very challenging since factors like rock type, heterogeneity, density, anisotropy, and porosity can affect the elastic wave velocity [22]. Based on these findings, it is feasible to compute tomographic maps. These representations offer a visual depiction of the internal condition of the structure or object under analysis, with distinct colours corresponding to varying travel times. The process for generating these tomographic images hinges upon the utilization of "travel times" and the coordinates of the examination points, which are input into tomographic algorithmic software. This software, in turn, calculates the paths of ultrasound inside the stone and determines the velocity within each constituent element of the surveyed cross-section, thereby generating tomograms that delineate variations in velocity across the stone. An illustrative example of such measurements is reported in Figure 8 [24].

Equation 3. Wave velocity formula.

$$V = \frac{L}{t - t_0}$$

V = ultrasonic wave velocity; L = measuring length; t = measured time; t_0 = time correction value.
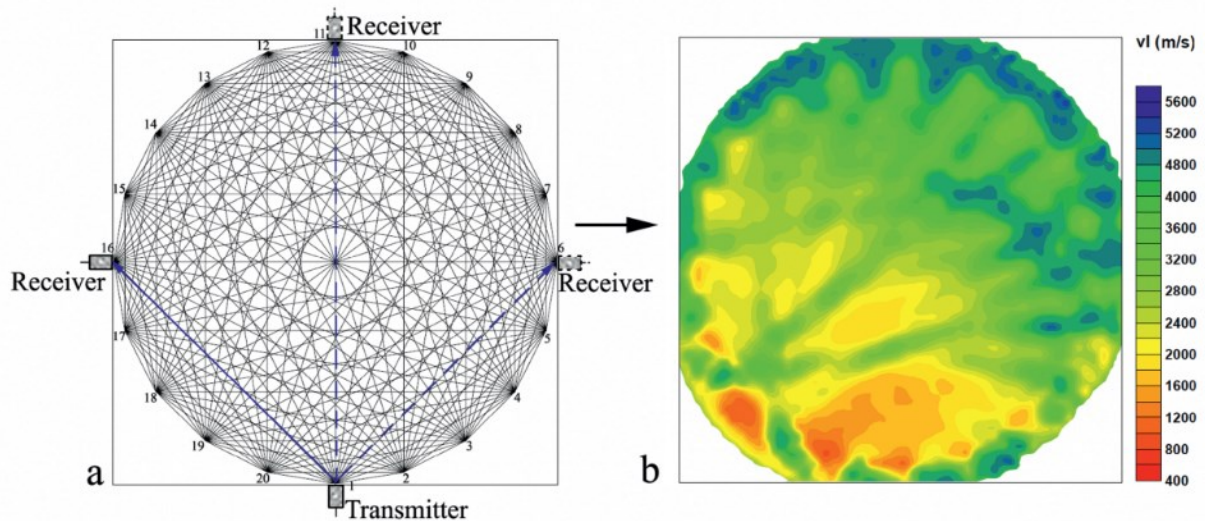
Figure 8. Ultrasonic tomography measurement. a) Scheme of the measurement points for the tomographic reconstruction of a section of a column; b) Tomogram for one stone section with the distribution of ultrasonic velocities (Ahmad, Pamplona, & Simon, 2014 [24]).

Additionally, even if the ultrasonic measurements use high frequencies and thus have high detecting power, this technique is more suitable for small objects. For bigger surfaces is indeed suggested to use sonic measurements which use the same principle as the ultrasonic ones. The difference stands in the use of a sonic hammer instead of a piezoelectric transmitter to produce the necessary waves. Consequently, to this last statement, in the case study of Geghard, it has been decided to use the ultrasonic method to overcome possible problems with the stone's high level of sensitivity. Here, it was used the *All-in One SYSTEM (SolGeo Instrument)* in 4 different areas of the Proshian family room walls and on the big basaltic octagonal column that sustains the section where the family crest is carved. The piezoelectric transmitter used for the survey has a high signal transmission power with a frequency of 55 kHz. Unfortunately, it was not possible to analyse bigger other parts of the room under investigation because of the necessity to carry out the measurements in relatively uninterrupted areas, including those pertaining to the architectural structure.

To reach more precise results, especially for the walls where it was not possible to measure big distances (lack of a signal that could be interpreted), the analyses were carried out in different coherent areas and then merged together. Figures 9 and 10 report the analysed wall areas and the correspondent paths: except from area "a" all the analysed walls were measured more than once with the same matrix of points as it is possible to understand from the images. In Figure 11, the octagonal column paths.
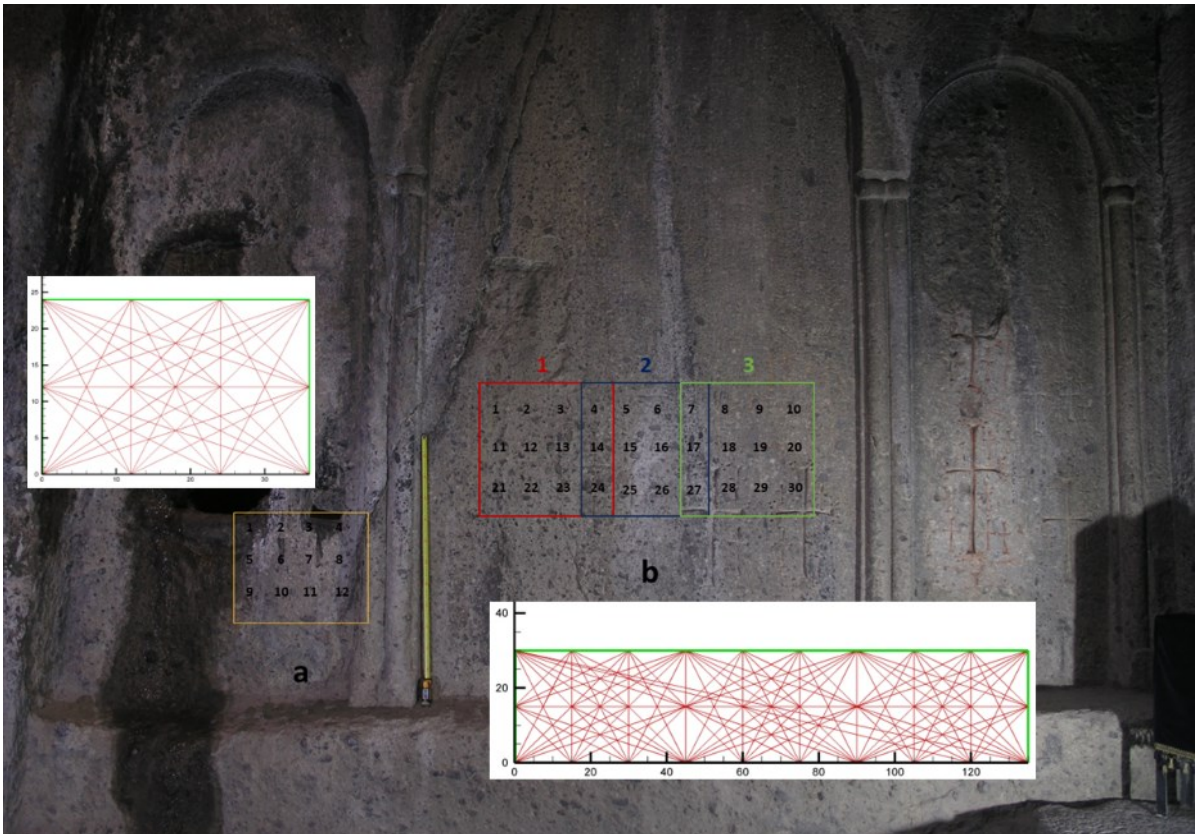
Figure 9. Points where the ultrasonic analyses were carried out on area "a" and "b" with the correspondent analysed paths.
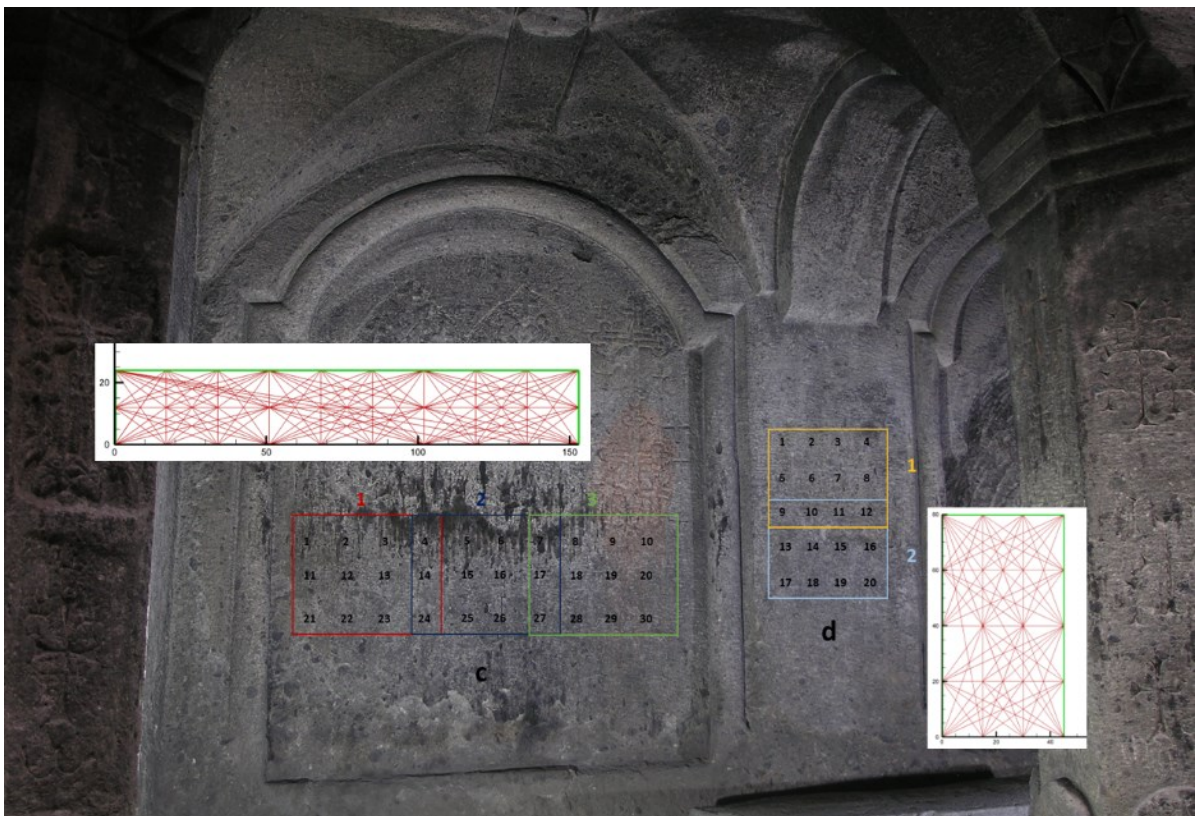

Figure 10. Points where the ultrasonic analyses were carried out on area "c" and "d" with the corresponded analysed paths.
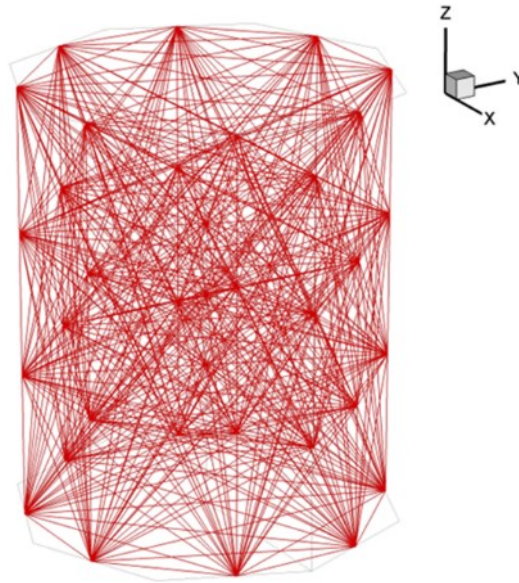
Figure 11. Column paths for ultrasonic analyses.

It is important to underline that to carry out this kind of measurement is suggested to be at least two persons so that one holds the source and the other holds the receiver. These measurements and the interpretation of the results were possible thanks to the collaboration with Dr Guido Driussi and Dr Matteo Morabito of *Arcadia Ricerche s.r.l, Venezia* who helped also with the development of the resulting tomographic maps.

2.6. Sampling campaign

In the monastery complex of Geghard where it was possible, some samples were taken with caution. With the use of gloves and a little blade, it was possible to collect a total number of 22 samples: 17 of them (from G_1 to G_17) from the Proshian family chamber, 2 of them (G_18 and G_19) from the upper chamber, and 3 of them from the outside (G_20 from a piece of cement used during the previous restoration work; G_21 and G_22 from the surrounding rocks). All of these samples were part of scaling processes, powders (efflorescences, black deposits, stone crumble and pigments) or waxes.

Hereafter, from Figure 12 to 15, the sampling points of the Proshian family room. In Figure 16 the remaining points on the upper chamber and the ones from the outside. A Table representing a macroscopic description of the different specimens collected and associated with the laboratory analyses conducted is also shown (Tab. 1).
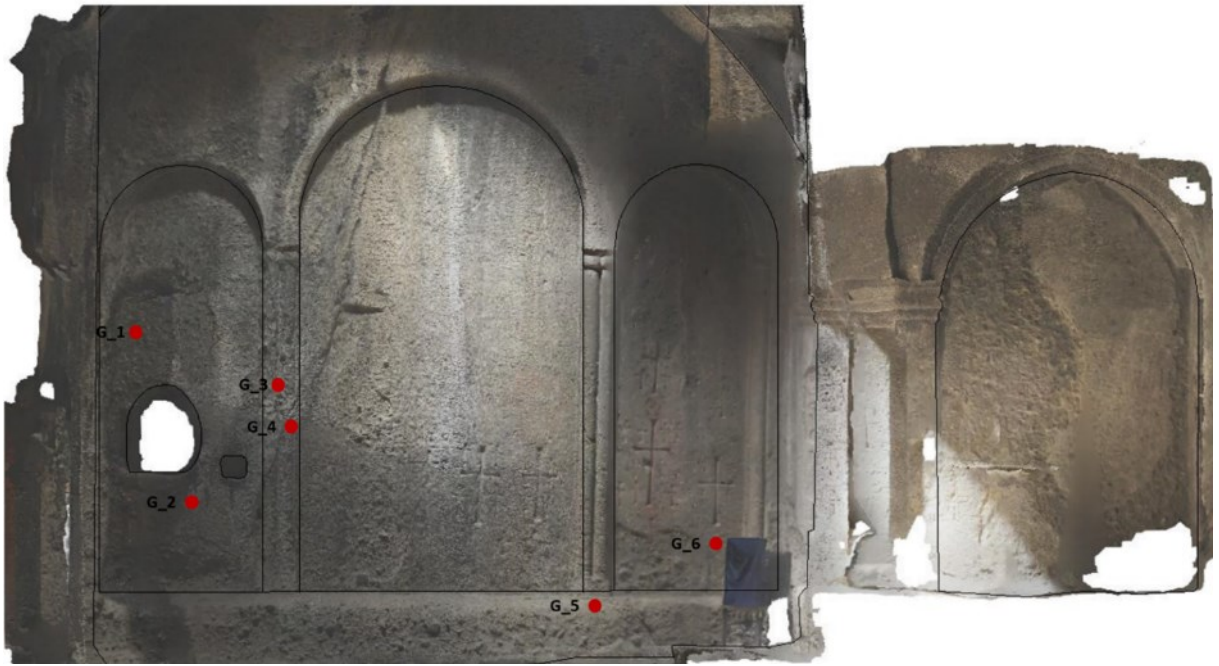
Figure 12. Sampled points on the Proshian family room western wall.

Figure 13. Sampled points on the Proshian family room eastern wall.

Figure 14. Sample points on the Proshian family room southern wall.

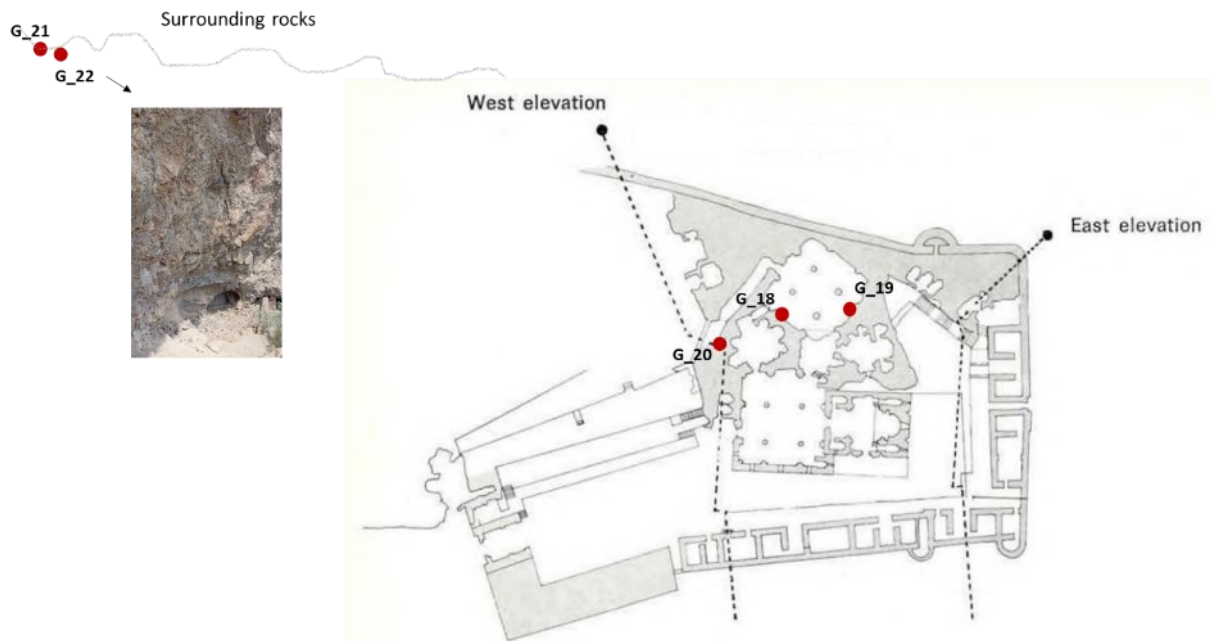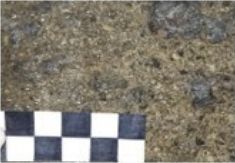*Figure 15. Sampled points on the Proshian family room northern wall.*
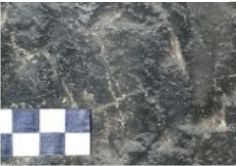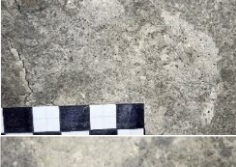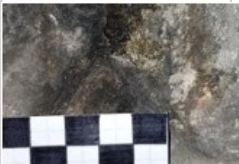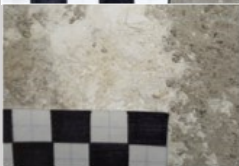
Figure 16. Sample points not belonging to the Proshian chamber (modified after Ara Stepanian, Telman Gevorgian, Edik Hovhannisian, Hratchia Gasparian & Edward Frangoulian, 1971).

Table 1. Descriptive table of the collected samples with indicated the respective laboratory analyses.

| | Sample name | Sample type | Sample picture | Laboratory analyses | | | | |
| | | | | *Microscope* | | *FTIR* | *Raman* | *Soluble salts* |
				TQ	Cross section			
Proshian room	G_1	Little piece of material		X		X		
	G_2	Little piece of material		X	X	X		
	G_3	Powder		X		X		
	G_4	Powder		X		X		
	G_5	Piece of rock		X	X			X
	G_6	Powder		X		X		

Room	Sample	Material	Image					
Proshian room	G_7	Powder		X		X		
	G_8	Powder		X		X		
	G_9	Little piece of material		X	X	X		
	G_10	Powder		X		X		
	G_11	Powder		X		X		
	G_12	Powder		X		X		
	G_13	Little piece of material		X	X	X	X	
	G_14	Powder		X		X		
	G_15	Wax		X				
	G_16	Powder		X		X		X
	G_17	Powder		X		X		

Location	Sample	Description	Image				
Upper room	G_18	Little piece of material		X		X	
	G_19	Powder		X		X	X
Outside	G_20	Little piece of material		X			
	G_21	Piece of rock		X		X	
	G_22	Piece of rock		X	X		

Considered the size of sample G_5 also XRD analyses were conducted powdering two different area that appeared different to the naked eye.

For sample G_11 also FTIR with KBr was conducted.

Laboratory analyses

Thanks to the samples that we were able to collect, laboratory analyses aimed at chemical identification of the compounds, were also possible (as shown in Table 1).

2.7. Microscopic observations

Microscopic observations of the sampled materials and powder are essential to examine their morphology and homogeneity. For this case study, all the samples were observed with the microscope Zeiss *Axiocam 208c with an Axioimager microscope* and magnifications from 1,25x to 9,45x (unit: μm). Where possible, the samples were observed both on the external part and in the internal part and some of these (G_2; G_5; G_9; G_13 and G_22), were also embedded in epoxy resin following the Normative CNR-ICR NorMal 14/83 [25] to try to observe in a better way the possible stratification and peculiarities.

2.8. Measurements of soluble salts

The presence of salts inside a material is one of the main issues that can affect the built Heritage [26]. Salts can, in fact, cause structural problems creating fractures, scaling, blistering and loss of materials in architectural structures. The mindfulness of the presence of salts can, for this reason, help us to understand if the actual degradation processes that are going on in the case under analysis, could be one of the actual causes.

In the case of Geghard monastery, 3 different samples (G_5, G_16 and G_19) were analysed to verify the presence of salts according to their conductivity values. The relationship between salt's conductivity and concentration is something ascertained: a higher concentration of salts means higher conductivity values [27, 28]. The samples were selected following the macroscopic and microscopic observations and in conformity with the quantity of sample present: G_16 and G_19 were selected because of their crystalline appearance; G_5 because it was the biggest stone sample collected that characterised the majority of areas of the Proshian family chamber. Moreover, of this last, it was possible to analyse both the inside and the external surface (indicated respectively with G_5_int and G_5_ext).

To measure salts conductivity, it was used *CRISON EC-Meter GLP 31* following the UNI Normal 13/83 [29]. The protocol requires 100 g of sample to be added to 100 ml of deionized water. However, since the quantity of G_16 and G_19 did not reach the 100 g planned it was used respectively 73 mg of sample with 73 ml of water and 87 mg of sample with 87 ml of water maintaining therefore the 1:1 proportionality. Yet, since this kind of measurement is micro-destructive, the samples G_16 and G_19 could not be used for further analyses.

2.9. Fourier Transform Infra-Red (FTIR) spectroscopy

FTIR spectroscopy is a reliable technique for studying especially organic and complex samples. In literature, there are many examples of the application of this technique for paintings or paper materials to analyse the varnishes present, particular pigments, inks etc.

Nevertheless, this methodology is becoming more and more used also for inorganic objects (stones, ceramics, glasses etc.). This is related to the well-established and comprehensive IR databases of minerals which have their characteristic IR vibrations. Moreover, also the possible degradation products present, could be identified with this technique [30]. Thus, it is possible to confirm that FTIR spectroscopy is a valid technique for studying both organic and inorganic materials [31].

During this thesis work, they were used two methodologies to study the selected samples: ATR-FTIR (Attenuated Total Reflectance) on the samples not previously treated and on pellets of KBr mixed with the samples. A *Bruker ALPHA II Fourier Transform IR Spectrometer* was used in both methods, with a spectral range from 4000 to 350 cm^{-1}, 4 cm^{-1} resolution and 64 scans for each sample. All the 22 samples were analysed with ATR (excluding G_15, G_19, G_5, G_21 and G_22). G_11 was also analysed with the KBr method to understand better some peculiar peaks that were not so clear with the ATR method. For sample G_3 also a salt extraction was carried out to divide the solid stone from the soluble salts to try to identify the different species more precisely. The data were then processed with *OPUS-Spectroscopy* software and *OriginPro* software.

The interpretation of the results was done through a comparison of different libraries present online (RRUFF, IRUG, DataBase, NIST) [32, 33, 34, 35], collected by the research group in Ca' Foscari University and results found in different scientific papers [36, 37, 38].

The choice of using especially the ATR method is because it permits the use of just a few milligrams of the sample, and it is a non-destructive technique. However, since stones show a high heterogeneity with the presence of different mineralogical compounds, ATR, given the small amount of analysed powder, requires a higher number of analyses in different samples to have representative results that can give an idea of the average composition of our specimen. KBr, on the other hand, even if it requires longer sample preparation and is a micro-destructive technique, gives spectra more representative of the sample, allowing better interpretations.

2.10. Raman spectroscopy

Raman spectroscopy is a very successful analytical technique for the characterization of many materials (organic, and inorganic) [39].

Just like FTIR spectroscopy, Raman spectroscopy is based on the vibrational modes of the sample molecules, which can be a fingerprint of the material or compound; this is one of the reasons why, today it is an established tool in Cultural Heritage investigations. Another advantage is its portability which allows the in situ analysis also on archaeological sites including outdoor applications. However, one big issue that we can encounter with Raman is its fluorescence sensitivity which can vanquish the scattering signal [40]. Also, the fact that the depth of the beam cannot be modulated, could be a source of problems leading to the misreading of the substrate especially if we are dealing with layered artefacts.

The Geghard samples that were analysed are G_21 and the surface black layer of sample G_13. For the analyses, it was used the *BRAVO Handheld Raman Spectrometer of Bruker* equipped with two laser *DuoLaser^(TM)* excitation (785 nm and 852 nm) that provides a high sensitivity across a broad spectral range. The resulting spectra were then processed with *OPUS-Spectroscopy* software and *OriginPro* software.

The choice of just these two samples was driven by the not-so-precise resulting signals, and the near absence of libraries for stone materials since this technique is much more used for paintings. Thus, for the result interpretation, reference was made to some publications [41, 42, 43, 44, 45] and the open libraries of RUFF [32] and IRUG [33].

2.11. XRD

XRD is the most reliable method for the identification of minerals or synthetic crystalline materials [39] which is possible through the resulting diffraction pattern. Although this technique is fundamental to complement chemical analyses like vibrational spectroscopy, it is not always possible to carry out due to the relative abundance of sample necessary (~0.5–1 g) [30]. For this reason, in the current work research, it was analysed just G_5 (the biggest sample that we were able to take). This specimen is considered to be representative of the stone constituent of the majority of the *Žamatoun* (Proshian family chamber) and we were able to collect it since it was found already detached from a broken zone where sometimes people sit. Its surface is characterized by a heterogeneous greyish appearance while in the bottom part a brighter matrix with small black mineral inclusions is observable (Fig. 17). Since during the preparation of the powder for the XRD analyses – where the sample was broken to reach its inner part – it was still noticed this big heterogeneity, it was decided to get 2 different powders: one from the softer, whiter, and predominantly type of stone/matrix and the other one from the darker and harder inclusions.
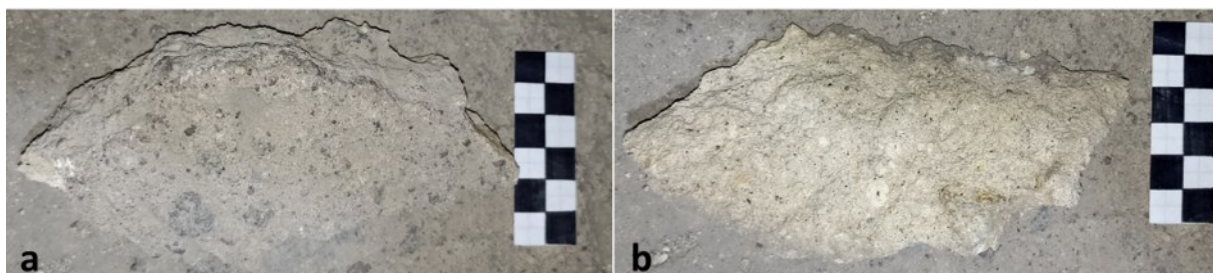

Figure 17. G_5 sample. a) surface of the sample; b) bottom part of the sample.

The analyses were carried out with a *PANalytical EMPYREAN XRD* and then interpreted manually with the help of *MATCH! Phase Analysis using Powder Diffraction* software and the

comparison of some scientific papers especially about basalt and tuff [46, 47, 48, 49], since these stones are one of the main materials present in Geghard according to Siegmund et. al [9]. *MATCH!* software was also used for the semi-quantitative results per each mineralogical phase.

[14] De Campos P., Appoloni C., Rizzutto M. A., Leite A. R., Assis R. F., dos Santos H. C., Silva T., Rodrigues C. L., Tabacniks M. H., Added N. A low-cost portable system for elemental mapping by XRF aiming in situ analyses. In: Applied Radiation and Isotopes. Elsevier; 2019

[15] Veneranda M., Irazola M., Pitarch A., Olivares M., Iturregui A., Castro K., Madariaga J. M. In-situ and laboratory Raman analysis in the field of cultural heritage: the case of a mural painting. In: Raman Spectroscopy. Wiley & Sons, Ltd.; 2014

[16] Camuffo D., MICROCLIMATE FOR CULTURAL HERITAGE Measurement, Risk Assessment, Conservation, Restoration, and Maintenance of Indoor and Outdoor Monuments. Third edition. Elsevier; 2019

[17] ICOMOS-ISCS. Illustrated glossary on stone deterioration patterns. 2008.

[18] Fitzner B, Heinrichs K, La Bouchardiere D. Damage index for stone monuments. In: Protection and Conservation of the Cultural Heritage of The Mediterranean Cities. 2002

[19] Tornari, V. Interferometric Quantification of the Impact of Relative. In: heritage. MDPI; 2023

[20] Muradov M., Kot P., Markiewicz J., Lapinski S., Tobiasz A., Onisk K., Shaw A., Hashim K., Zawieska D., Mohi-Ud-Din G. Non-destructive system for in-wall moisture assessment of cultural. In: Measurements. Elsevier; 2022

[21] Ribeiro T., Oliveira D. V., Bracci S. The use of contact sponge method to measure water absorption in earthen heritage trated with water repellents. In: International Journal of Architectural Heritage. 2020

[22] Fais S., Cuccuru F., Ligas P., Casula G. Integrated ultrasonic, laser scanning and petrographical characterisation of carbonate building materials on an architectural structure of a historic building. In: Bulletin of Engineering Geology and the Environment. Springer Nature; 2015

[23] Vary A. Ultrasonic measurement of material properties. In: Ultrasonic Characterization of Material Properties. NTRS; 1980.

[24] Ahmad A., Pamplona M., Simon S. Ultrasonic testing for the investigation and characterization of stone – a non-destructive and transportable tool. In: Studies in Conservation. 2014

[25] Normative CNR-ICR NorMal 14/83 – Sezioni Sottili e Lucide di Materiali Lapidei: tecnica di Allestimento

[26] Germinario L., Oguchi C. T. Underground salt weathering of heritage stone: lithological and environmental constraints on the formation of sulfate efflorescences and crusts. In: Journal of Cultural Heritage. Science direct; 2021

[27] Widodo C. S., Sela H., Santosa D. R. The effect of NaCl concentration on the ionic NaCl solutions electrical impedance value using electrochemical impedance spectroscopy methods. In: THE 8TH ANNUAL BASIC SCIENCE INTERNATIONAL CONFERENCE: Coverage of Basic Sciences toward the World's Sustainability Challenges. 2018

[28] Polle A., Chen S. On the salty side of life: molecular, physiological and anatomical adaptation and acclimation of trees to extreme habitats. In: Plant Cell and Environment. John Wiley & Sons Ltd; 2014

[29] UNI Normal 13/83 – Dosaggio dei Sali Solubili

[30] Liu G.-L., Kazarian S. G. Recent advances and applications to cultural using ATR-FTIR spectroscopy and ATR-FTIR spectroscopic imaging. In: Royal society of chemistry. 2022

[31] Glavcheva Z. I., Yancheva D. Y., Kancheva Y. K., Velcheva E. A., Stamboliyska. B. A. Development of FTIR spectra database of reference art and archaeological materials. In: Bulgarian Chemical Communications. 2014

[32] rruff.info (Internet). RRUFF (accessed on: September 2023). Available at: https://rruff.info/

[33] irug.org (Internet). IRUG Infrared & Raman Users Group. 1993 (accessed on: September 2023). Available at: http://www.irug.org/

[34] spectrabase.com (Internet). SpectraBase, Wiley & Sons (accessed on: September 2023). Available at: https://spectrabase.com/

[35] webbook.nist.gov (Internet). NIST Chemistry WebBook, NIST National Institute of Standards and Technology U.S. Department of commerce (accessed on: September 2023). Available at: https://webbook.nist.gov/chemistry/name-ser/

[36] Lacheha, A., Mertah O., Kherbeche A., & Hassoune H. Utilization of phosphogypsum in CO2 mineral sequestration by producing potassium sulphate and calcium carbonate. In: Materials Science for Energy Technologies. KeAi Chinese roots global impact; 2020

[37] Janek,M., Bugár I., Lorenc D., Szöcs V., Velič D., Chorvát D. Terahertz Time-Domain Spectroscopy of Selected Layered Silicates. In: Clays and Clay Minerals. 2009

[38] Santo A. P., Benedetto F. D., Garzonio C. A., Pecchioni E., Salvatici T., Coppola M. Stone Architectural Decoration in Burji Era: The Northern Mausoleum in the Khanqah of Al-Nasir Faraj Ibn Barquq (Cairo). Contribution to the Knowledge and Conservation Assessment. In: heritage. MDPI; 2021

[39] Brunetti B., Miliani C., Rosi F., Doherty B., Monico L., Romani A., Sgamellotti A. Non-invasive Investigations of Paintings by Portable Instrumentation: The MOLAB Experience. In: Springer, Analytical Chemistry for Cultural Heritage. Mazzeo R.; 2016

[40] Casadio F., Daher C., Bellot-Gurlet L. Raman Spectroscopy of cultural heritage Materials: Overview of Applications and New Frontiers in Instrumentation, Sampling Modalities, and Data Processing. Springer, Analytical Chemisty for Cultural Heritage. Mazzeo R.;2016

[41] Gunasekaran S., Anbalagan G., Pand S. Raman and infrared spectra of carbonates of calcite structure. In: Raman Spectroscopy. Wiley & Sons, Ltd; 2006

[42] Xie T., Osinski G. R., Shieh S. R. Raman study of shock effects in lunar anorthite from the Apollo missions. In: Meteoritics & Planetary Science. MET; 2021

[43] Pawlyta M., Rouzaud J.-N., Duber S. Raman microspectroscopy characterization of carbon blacks: Spectral analysis and structural information. In: Carbon. 2014

[44] Coccato A., Jehlicka J., Moens L., Vandenabeel P. Raman spectroscopy for the investigation of carbon-based black pigments. In: Raman Spectroscopy. Wiley & Sons, Ltd; 2015

[45] Parc R. L., Champagnon B., Dianoux J., Jarry P., Martinez V. Anorthite and CaAl2Si2O8 glass: low frequency Raman spectroscopy and neutron scattering. In: Non-Crystalline Solids. 2003

[46] Chen X., Zhang Y., Hui, D., Chen M., Wu Z. Study of melting properties of basalt based on their mineral components. In: Composites Part B: Engineering. 2017

[47] Yilmaz S., Özkan O. T., Günay V. Crystallization kinetics of basalt glass. In: Ceramics International. 1996

[48] Alzboon K. K., Al Smadi B. M., Al-Khawaldh S. Natural Volcanic Tuff-Based Geopolymer for Zn Removal: Adsorption Isotherm, Kinetic, and Thermodynamic Study. In: Water Air and Soil Pollution. 2016

[49] Senila M., Neag E., Cadar O., Hoaghia M.-A., Roman M., Moldovan A., Hosu A., Lupas A., Kovacs E. D. Characteristics of Volcanic Tuff from Macicasu (Romania) and Its Capacity to Remove Ammonia from Contaminated Air. In: *molecules*. Advanced Analytical Techniques in Environmental Chemistry; 2022

3. Results and discussion

Chapter 3: "Results and discussion" follows the same scheme of "Materials and methods". Thus, the surveys carried out in situ are divided from the laboratory analyses.

<u>In situ analyses</u>

3.1. Environmental monitoring

The result of environmental monitoring of the Proshian family chamber is reported in Figure 18.
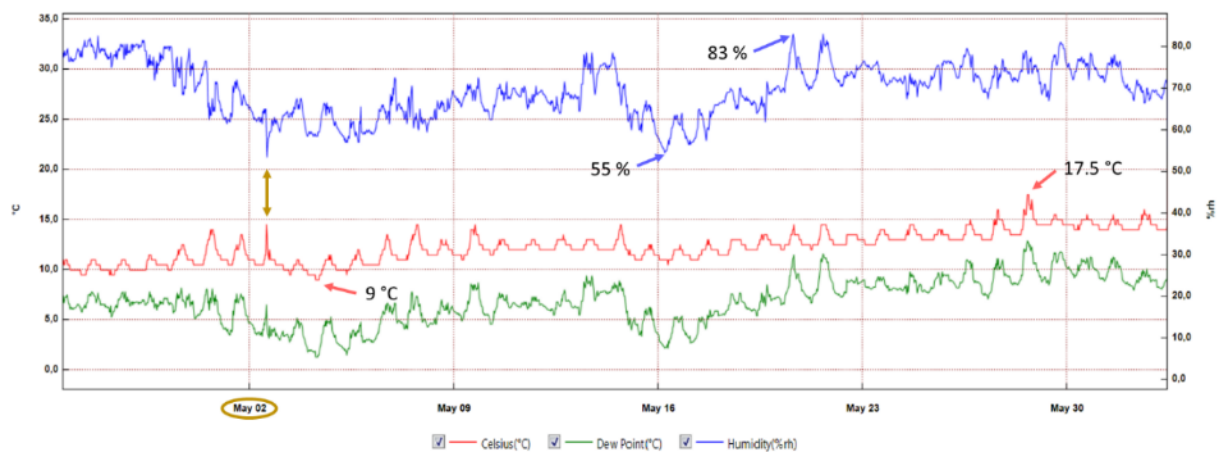

Figure 18. Environmental monitoring results from 04/25/2023 to 06/02/2023.

Here it is possible to observe how the temperature swings between a minimum of 9 °C and a maximum of 17, 5 °C and the relative humidity values go from a minimum of 55 % to 83 %. These numbers are coherent with what was expected since the analysed room is carved into the rock, and inside the monastery, there is no heating system. Sometimes indeed happens that in operating churches heating systems are used and these can create a lot of differences, especially between daylight and night depending on when the heating is turned off/on [50].

For these reasons, the oscillations present in Geghard could be associated with the number of tourists inside the room, the time of the day and the external weather. Between 4 p.m. and 6 p.m., it is possible to observe higher and sharp peaks that could be related to the fact that every day the monastery hosts and celebrates one or two weddings that inevitably bear a lot of people all at once. Lower temperatures are observable during the first hours of the morning when the monastery opens to the public (Between 7 and 9 o'clock a.m.), while they seem stable during the closing time with some exceptions where the temperatures stay constant between midnight and midday. Even the dew point behaviour could correspond to the possible number of visitors

as it increases at the busiest visiting hours. Crowded rooms are indeed known to have more moisture content since people produce moisture while breathing [16]. Despite that, the condensation conditions are never reached. Moreover, it seems that the temperature is slightly increasing over the months which would be coherent with external weather conditions of that period. We can also notice how usually higher temperatures mean higher RH values, except from the case on May 02 where this behaviour is evidently the opposite. This difference can possibly be explained since that day, the datalogger was removed for 1-2 hours once it was found out that the other one disappeared, and it was considered for a moment to interrupt the measurements.

3.2. Visual survey: degradation map and "degradation indicators"

In the resulting table of the degradation indicators (Tab. 2), the selected pictures used for the comparison between 2018 and 2023 situation, are shown with the respective values. This evaluation, necessary to understand the evolution over time of the selected case study, highlights what seems to be a stable situation. There are not such great differences in 5 years as it is possible to understand from Table 3. This table shows graphically the situation, allowing a prompt understanding. Moreover, in Table 3b is reported the close-up of the Linear Damage Indicator and of the Progressive Damage Indicator. The slight differences visible are related especially to changes of colours or loss of material like in the case of "Photo 9" where a keen eye can notice that a piece of the rock above the stairs, close to the grid, fell.

Table 2. Table of the degradation indicators associated with the pictures of 2018 and 2023.
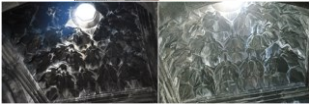
		D.I. 0		D.I. 1		D.I. 2		D.I. 3		D.I. 4		D.I. 5		DI (linear)		DI (progressive)	
		2018	2023	2018	2023	2018	2023	2018	2023	2018	2023	2018	2023	2018	2023	2018	2023
Photo 1		0	0	0	0	10	10	30	30	10	10	50	50	4,0	4,0	4,15	4,15
Photo 2		0	0	0	0	5	5	10	5	40	45	45	45	4,3	4,3	4,33	4,37
Photo 3		0	0	5	0	0	5	30	30	30	30	35	35	3,9	4,0	4,04	4,06
Photo 4		5	5	40	20	10	20	35	45	10	10	0	0	2,1	2,4	2,36	2,58
Photo 5		0	0	5	5	30	10	30	35	15	30	20	20	3,2	3,5	3,37	3,66
Photo 6		15	15	5	0	10	15	30	30	25	25	15	15	2,9	3,0	3,30	3,32
Photo 7		0	0	0	0	5	5	60	60	35	35	0	0	3,3	3,3	3,35	3,35
Photo 8		0	0	0	0	15	10	40	45	30	30	15	15	3,5	3,5	3,57	3,61
Photo 9		0	0	5	5	0	0	20	5	30	20	45	70	4,1	4,5	4,23	4,60

Table 3. Graphical representation of the resulting comparison between the 2018 and 2023 situation. a) the degradation indicators from 1 to 5; b) resulting linear and progressive damage indices.
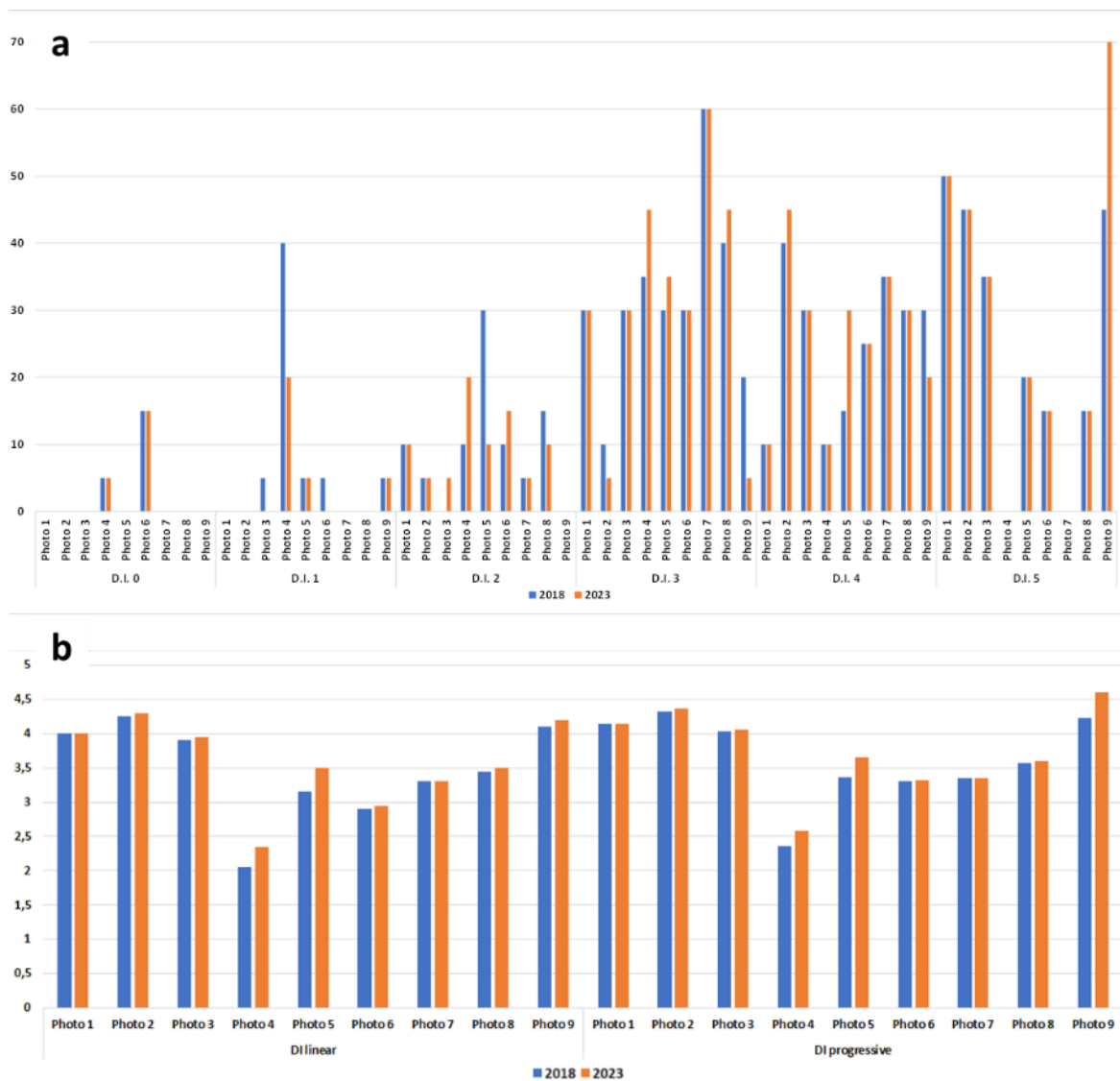
The degradation maps depicting the vertical surfaces of the analysed room are presented from Figure 20 to Figure 24. A comprehensive legend is provided in Figure 19 illustrating various patterns along with brief descriptions [17], their corresponding names, and representative images, all arranged alphabetically. The pictures used in the legend were both macroscopic and, where possible, microscopic with UV light and visible light. Notably, not always the microscopic pictures coincide with the macroscopic ones. This is because the selected images are chosen to be representative just of the kind of degradation pattern in general.

In each map is then reported a less detailed legend to promptly understand the situation.

Macro-picture	Micro-picture VIS	UV	Degradation pattern's name	ICOMOS definition	Annotations
			Blistering	Separated, air-filled, raised hemispherical elevations on the face of stone resulting from the detachment of an outer stone layer. This detachment is not related to the stone structure.	
			Chalk Graffiti	Engraving, scratching, cutting or application of paint, ink or similar matter on the stone surface.	Here it was deliberately specified «chalk» to distinguish these graffitis from those made with wax.
			Colouration	Change in hue, value and/or a gain in chroma.	
			Crack	Individual fissure, clearly visible by the naked eye, resulting from separation of one part from another.	
			Cut	Loss of material due to the action of an edge tool. It can have the appearance of an excavated cavity, an incision, a missing edge, etc...	
			Erosion	Loss of original surface, leading to smoothed shapes.	This term was used to distinguish whenever there were other and more intensive mechanical damages related to mechanical loss.
			Improper intervention	Intervention with the aim of restoring the concerned object, which, however, is not appropriate. It may be due to the application of inappropriate materials (colour and texture clearly different from the original material)	TERM NOT PRESENT IN THE ICOMOS GLOSSARY
			Loss of Matrix	Partial or selective elimination of the stone matrix, resulting in protruding compact stone components.	
			Missing part	Empty space, obviously located in the place of some formerly existing stone part.	
			Moisture area	Corresponds to the darkening (lower hue) of a surface due to dampness.	This term was used as a general term for those surfaces where the water presence is evident. Thus also for areas that were actually wet.
			Salt encrustation	Compact, hard, mineral outer layer adhering to the stone. Surface morphology and colour are usually different from those of the stone.	«Salt» was deliberately specified to highlight the presence of an adherent natural white material
			Scaling	Detachment of stone as a scale or a stack of scales, not following any stone structure and detaching like fish scales or parallel to the stone surface. The thickness of a scale is generally of millimetric to centimetric scale.	
			Staining	Kind of discolouration of limited extent and generally of unattractive appearance.	
			Rounding	Preferential erosion of originally angular stone edges leading to a distinctly rounded profile. Rounding can especially be observed on stones which preferably deteriorate through granular disintegration	
			Wax deposit	Accumulation of exogenic material of variable thickness.	The term «wax» is used to specifically indicate that this kind of deposit is often a thick adherent layer and nothing like a dust deposit for instance.
			Wax graffiti	Engraving, scratching, cutting or application of paint, ink or similar matter on the stone surface.	Here it was deliberately specified «wax» to distinguish these graffitis from those made with a chalky material.

Figura 19. General legend used for the identification of the degradation patterns highlighted in the degradation maps.

On the following maps (Figs. 20-24) it was decided to emphasize the most evident degradation processes within Proshian family room. The whole room, indeed, is almost entirely subjected to degradation. Salts, for instance, are almost everywhere as incrustation or efflorescences. For this reason, we marked this degradation pattern only when it was concentrated in specific areas.

Also, biological colonization (such as the presence of spider webs or little nests of dead insects), some sort of crusts not well identified, other kinds of deposit (chewing gum stuck to the surface) or crumbling (especially from the points where the samples were then collected) can be occasionally observed.

Furthermore, the degradation pattern that was identified as scaling, if decontextualized might resemble erosion or differential erosion, yet upon comprehensive examination of the entire complex surface, one can discern the presence of detached layers akin to scales.
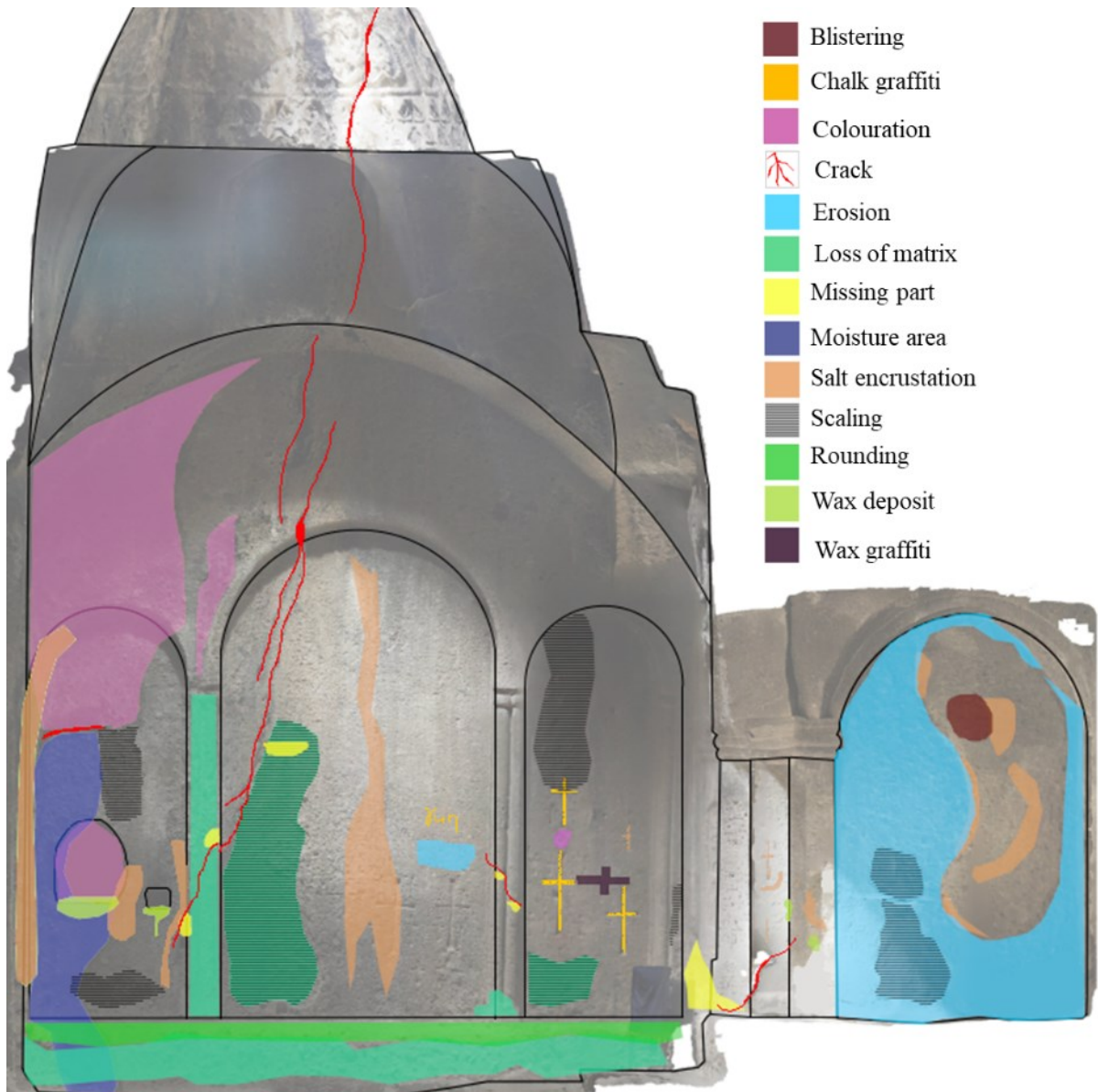

Figure 20. Degradation map correspondent to the western wall of the Proshian family room.
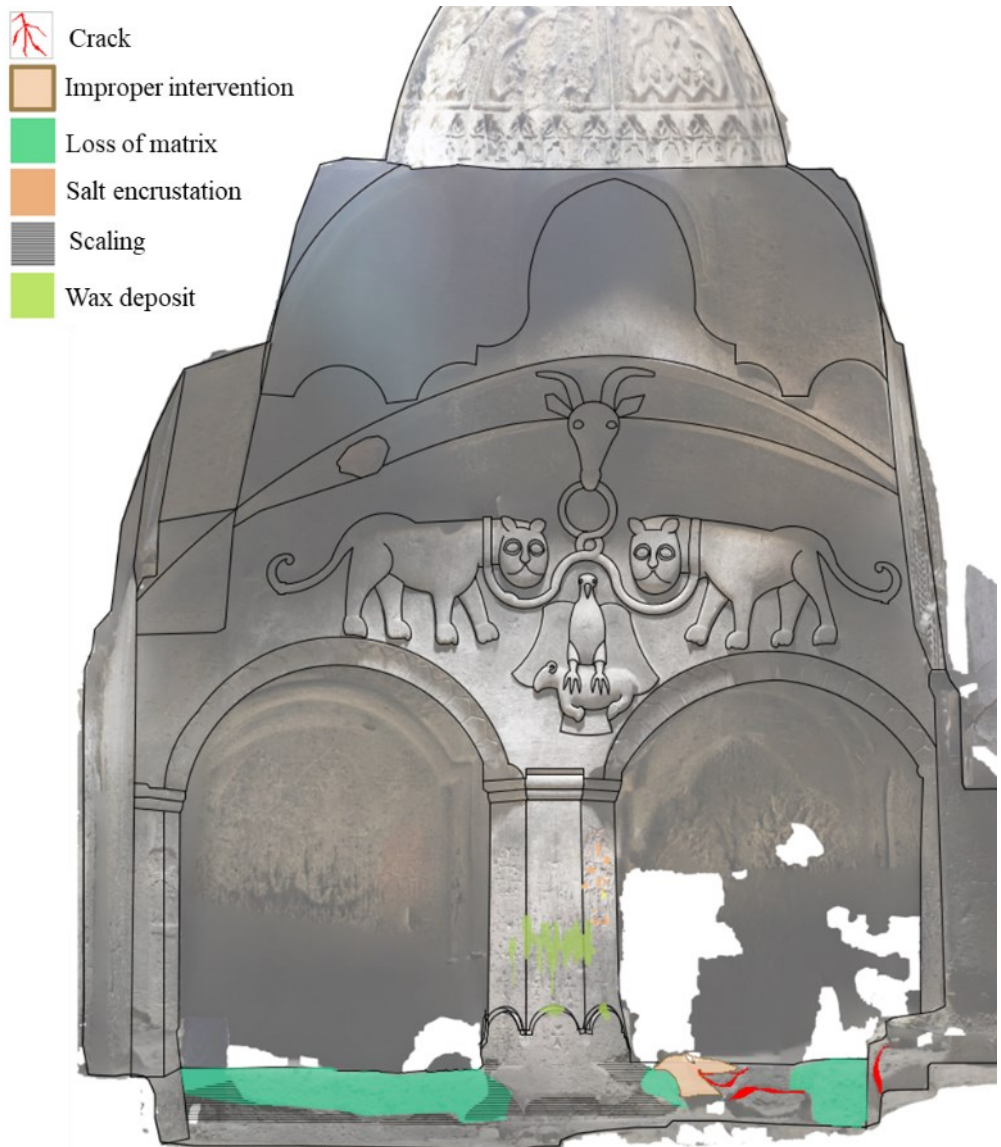
Figure 21. Degradation map of the octagonal colomun and base of the Proshian family room (view from the centre of the chamber.

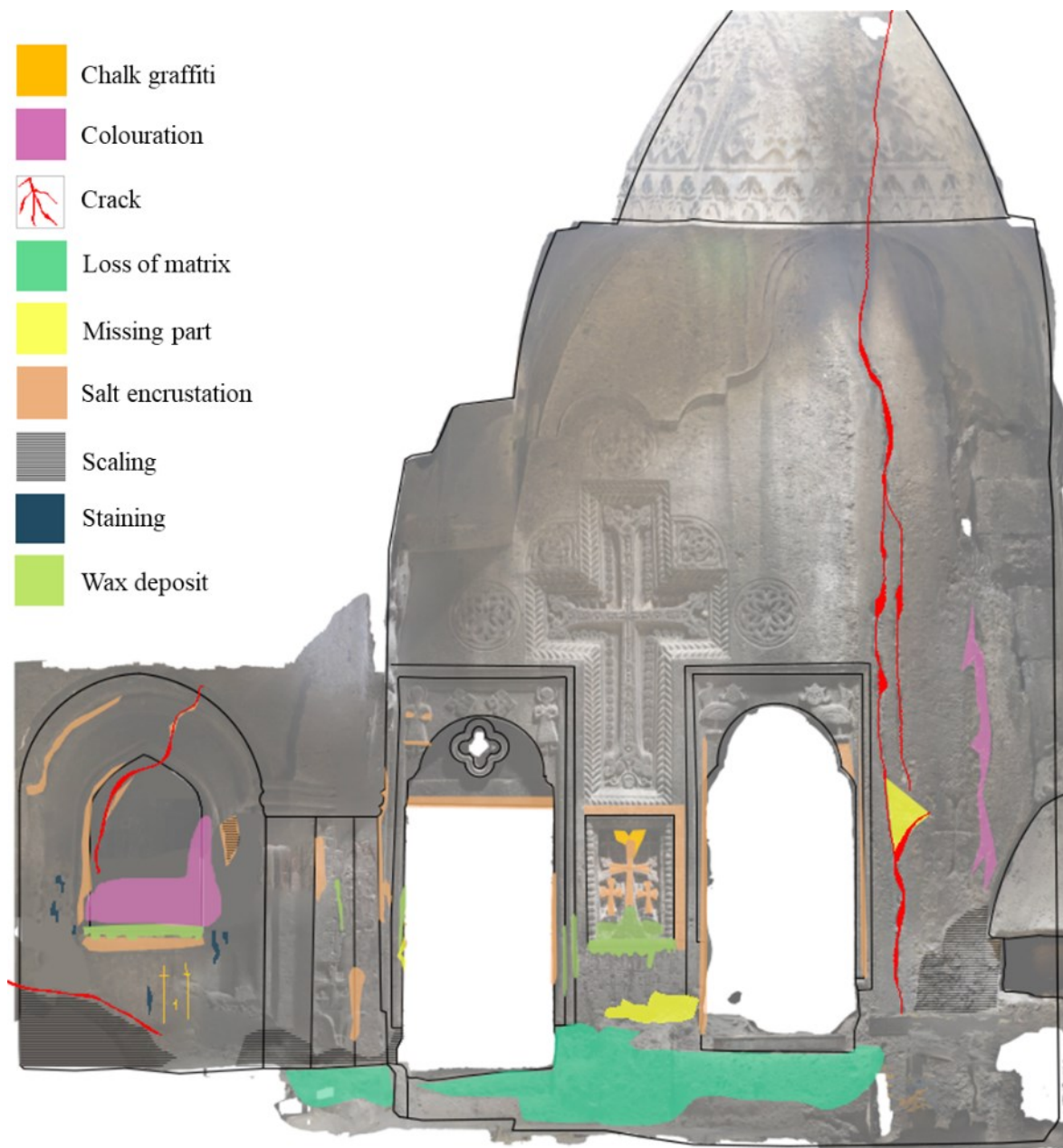*Figure 22. Degradation map of the northern wall of the Proshian family room.*

Figure 23. Degradation map of the eastern wall of the Proshian fam_ilt room
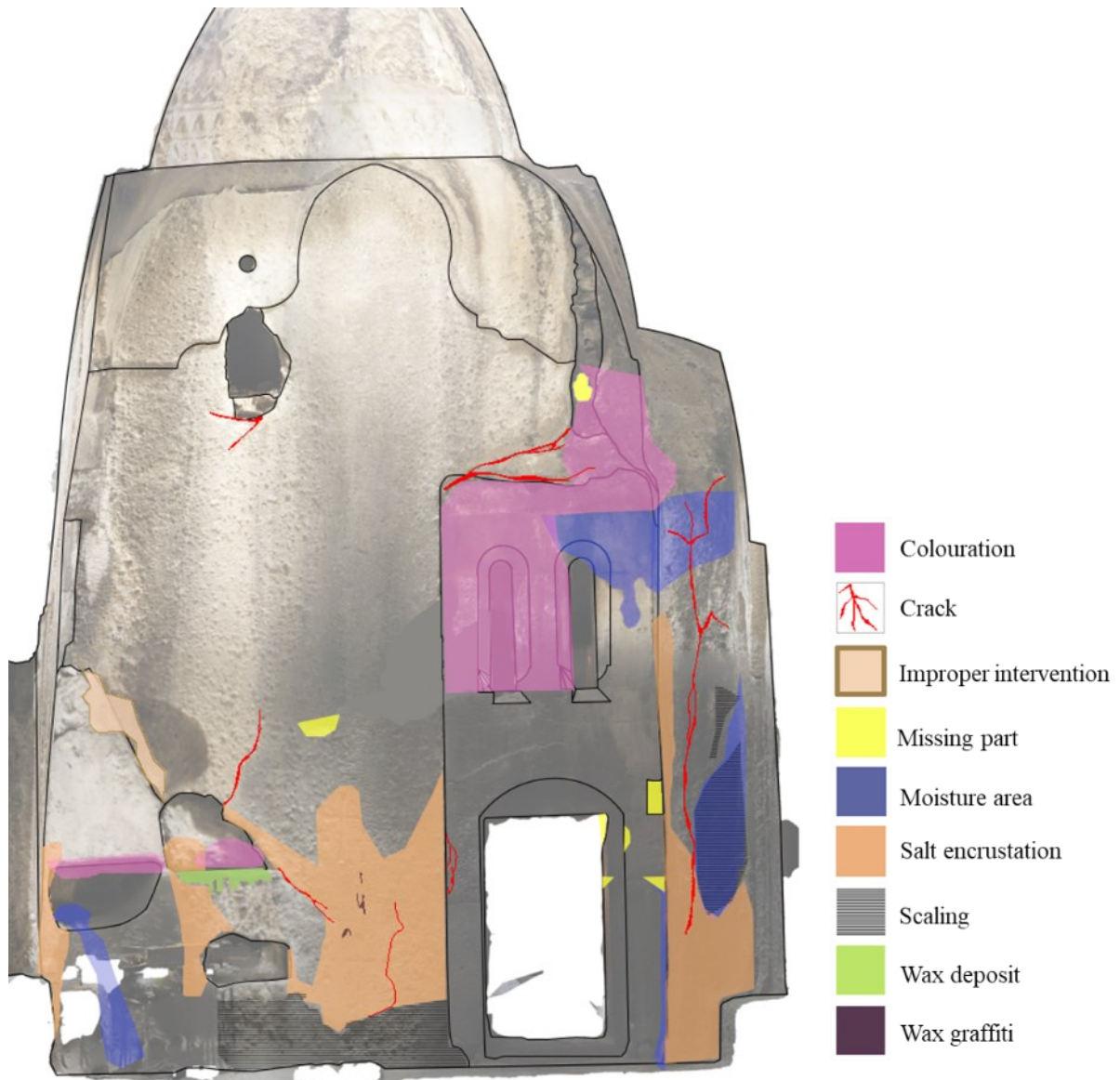
Figure 24. Degradation map of the southern wall of the Proshian family room.

From these maps, it is possible to notice a wide variety of degradation patterns, some more particular than others, so it was not always practicable to strictly follow the ICOMOS glossary [17]. Scaling is evident on all walls alongside salt encrustation and wax deposits. Additionally, it is possible to observe, especially on the sculpted sections, variations in surface height, with lower zones exhibiting a considerably more critical condition than higher zones.

3.3. Surface Humidity

The *Protimeter MMS2* results were reported in colour maps (Figs. 25-29 and 31) as already anticipated in the previous chapter (Chpt. 2.3.). Hither were used different approximated scales

according to the wall analysed and its own values results. This choice was made to highlight the differences present among the wall points measured.

In the map corresponding to the Proshian family's west wall (Fig. 25) the minimum value is equal to 152 and the maximum to 287. According to the values of the manual of the instrument used, we thus have that between 152 to 170 we should deal with dry conditions, from 170 up to 200 we should be in a risky situation and for those that go from 170 to 287 we should have a wet area. In this map, some points are more evident, and we can notice how there is not a gradient difference between the bottom and high parts. It does not seem that there is a relationship with rising damps but there are located areas that suffer more than others. Anyway, these results seem to be odd since do not really reflect the real situation, for instance: in the left arc beneath the "window" there is constantly an evident moisture area with water that comes out from an upper fracture; theoretically, the value result should be equal to the maximum (999), but this is not clearly happening even though more measurements were taken. This is just an example, but it was one of the main reasons why the efficiency of the used tool was questioned.
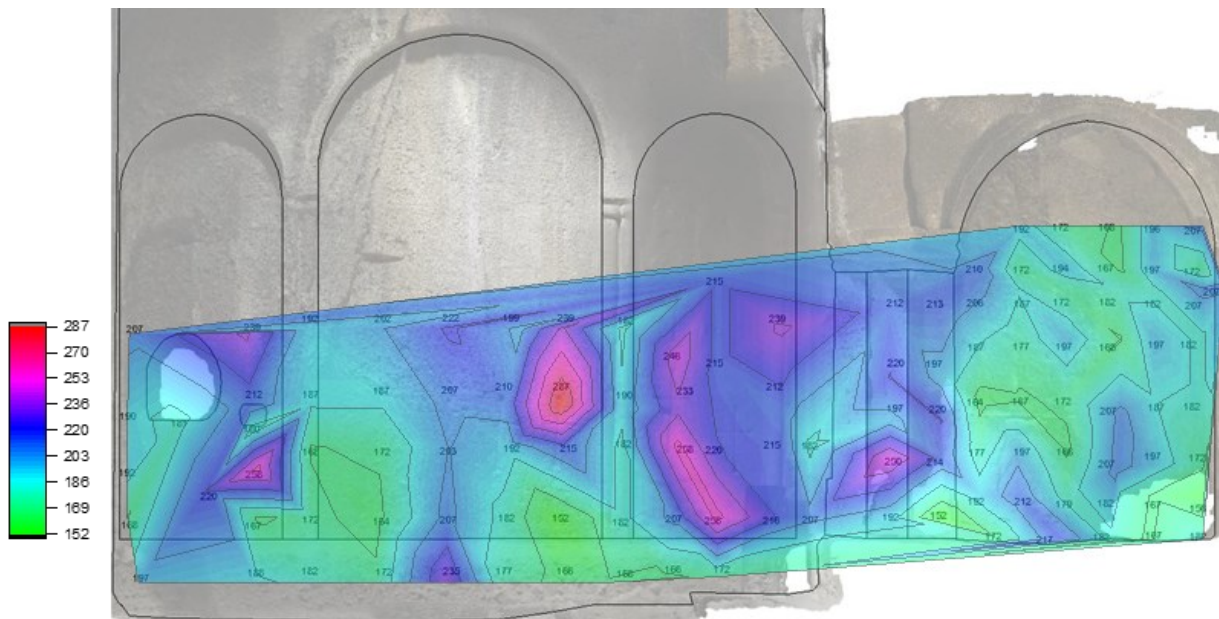

Figure 25. Colour map based on the surface humidity results with Protimeter MMS2 on the western wall of the Proshian family room.

In Figure 26, the map corresponding to the columns and the base to the upper part of the Proshian family's chamber is reported. Here the minimum value reached is 156 and the maximum is 646 (in the left semi-column). All the lower areas seem in good condition for what concerns the homogeneity but, according to the instrument specification, there are some points where the correspondent value is considered to be at risk or wet. Actually, the stones which compose the columns, and the base were probably subjected to a different kind of work and

seem to be a different material too. It is reminded that in accordance with the few literature sources available about the Geghard monastery [9, 10], there should be two different main kinds of stones: tuff and basalt. As specified by Wedekind et al., each of these two kinds of rocks is differentiated in turn into two different typologies: one with higher porosity values and one with lower porosity values. For basalt, the lower porosity kind has values equal to 17,4 % while the other one has values equal to 23,5 %. For tuff, the lower one corresponds to 30 % in porosity while the higher one corresponds to 38,8 %. Even though there are no sources that really indicate which one is what, we can suppose that the basalt is the one in correspondence with the column and the sculpted zones since it is characterized by a darker colour and more visible compactness. The tuff instead could be the one characterizing the base featured by a visible heterogeneity.
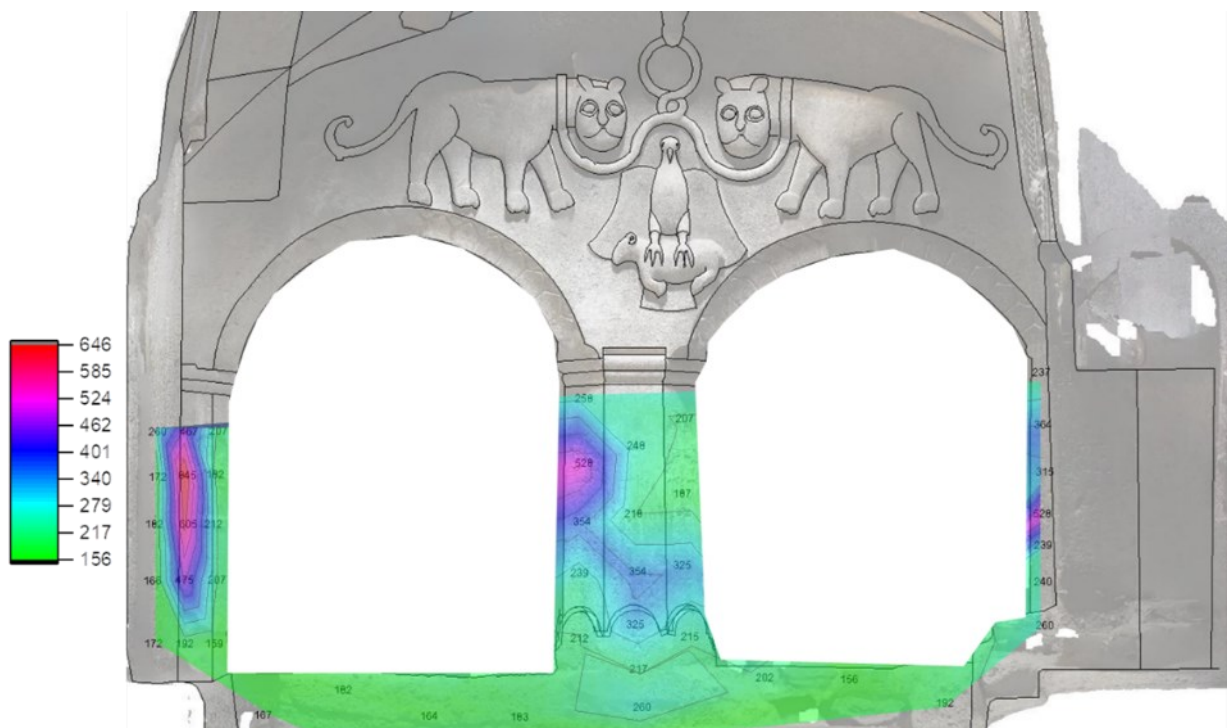

Figure 26. Colour map based on the surface humidity results with Protimeter MMS2 on the columns and base of the Proshian family room (view from the centre of the chamber).

In the northern wall (Fig. 27), the surface humidity results go from 120 up to 287. Therefore, compared to the other areas, it is possible to observe some localized higher points but a distribution much more homogeneous. This may be related to the fact that this part is adjoined directly and only with the live rock, and it is less in contact with the visitors who tend to stay around the centre of the room; something that in the other areas – even though some still carved – does not occur considering that they are adjacent to other rooms and are strictly in contact with visitors too.
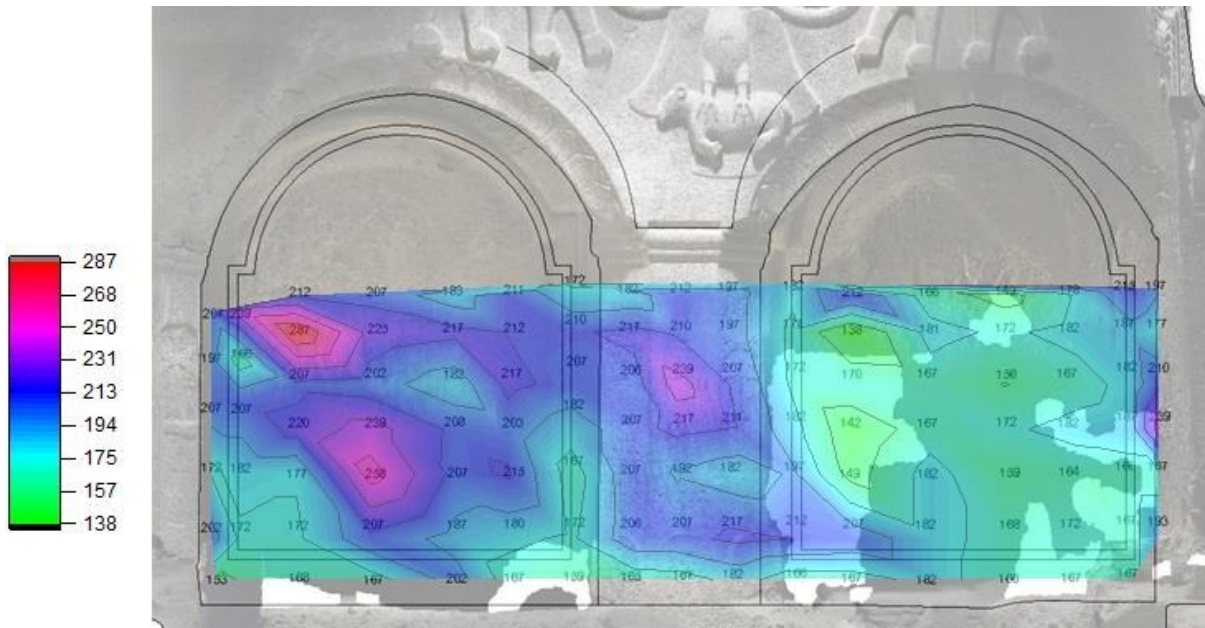
Figure 27. Colour map based on the surface humidity results with Protimeter MMS2 on the nothern wall of the Proshian family room.

Confirming what has just been said in Figure 28 we can observe the colour map of the eastern wall of the Proshian family chamber which is adjacent to another room of the monastery. In fact, the resulting values measured go from 149 to 528: a bigger difference compared to the previous result of the northern wall (Fig. 27). Localized higher points are still present, and just few points are under 170 (value that marks the "at risk" situation).
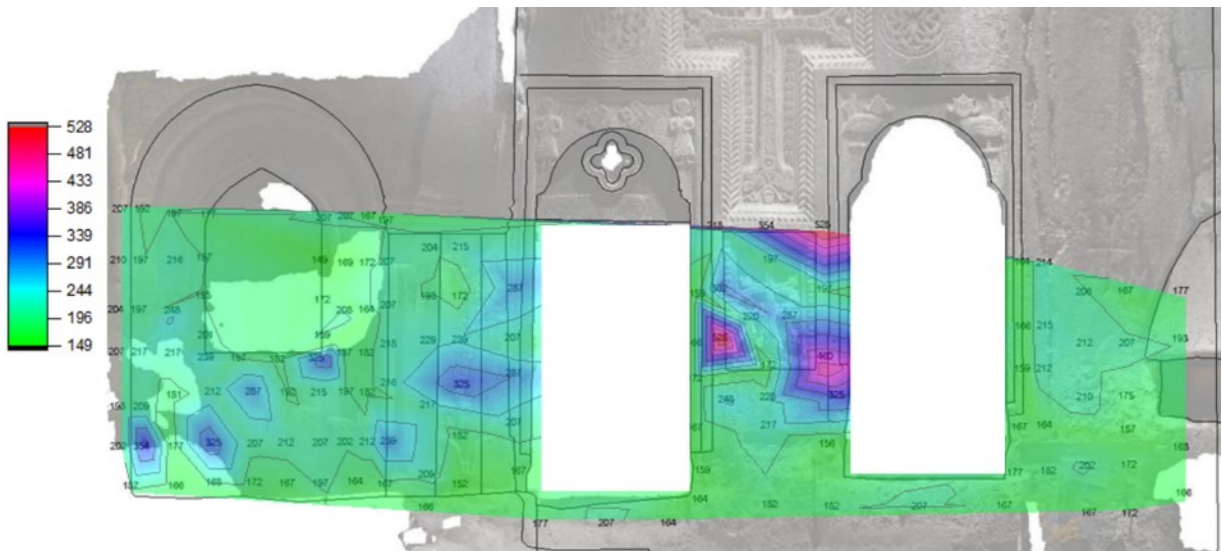

Figure 28. Colour map based on the surface humidity results with Protimeter MMS2 on the eastern wall of the Proshian family rooml.

In the southern wall map (Fig.29 a) the lowest value is 136 and the higher is equal to 354 reached in both more red points that stick out. Here there are more discontinuities in the measurements because of the architectural structure used in the past such as an old fireplace and a place underneath it more carved forming a recess, and an old safety deposit box (see Figure 29b).
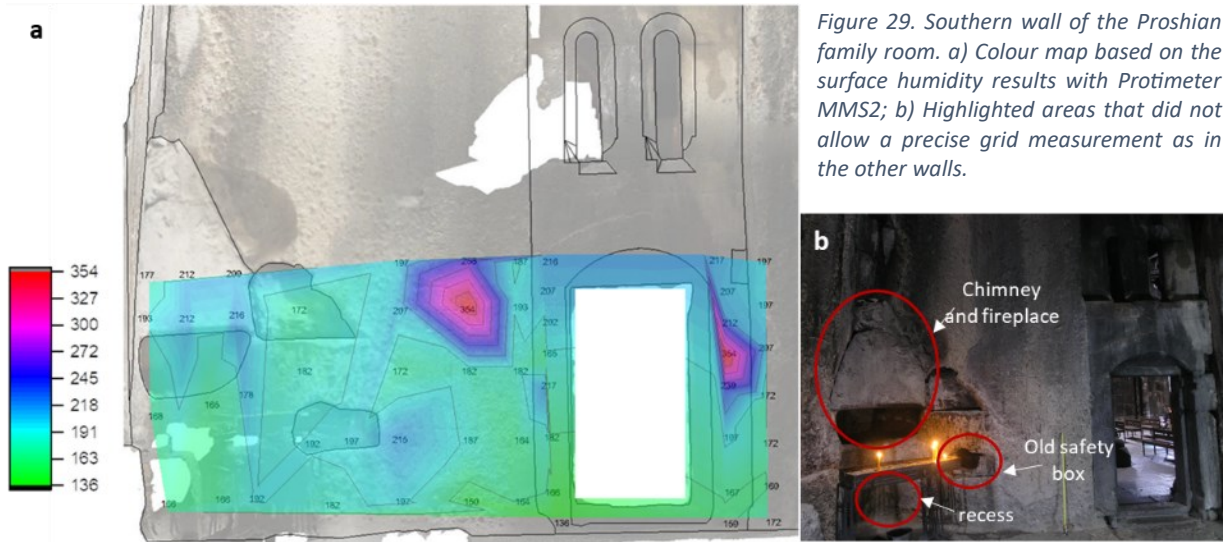

Figure 29. Southern wall of the Proshian family room. a) Colour map based on the surface humidity results with Protimeter MMS2; b) Highlighted areas that did not allow a precise grid measurement as in the other walls.

Finally, in the octagonal column (Fig. 30), the humidity measurement values go from 145 to 558. Immediately visible is the difference between the front and the back of the column. The side facing the centre of the chamber (front) has higher values compared to the other side which is probably more protected from convection motions and tourists. This behaviour could be a sign related to the microclimate to which the chamber can be subjected [16].
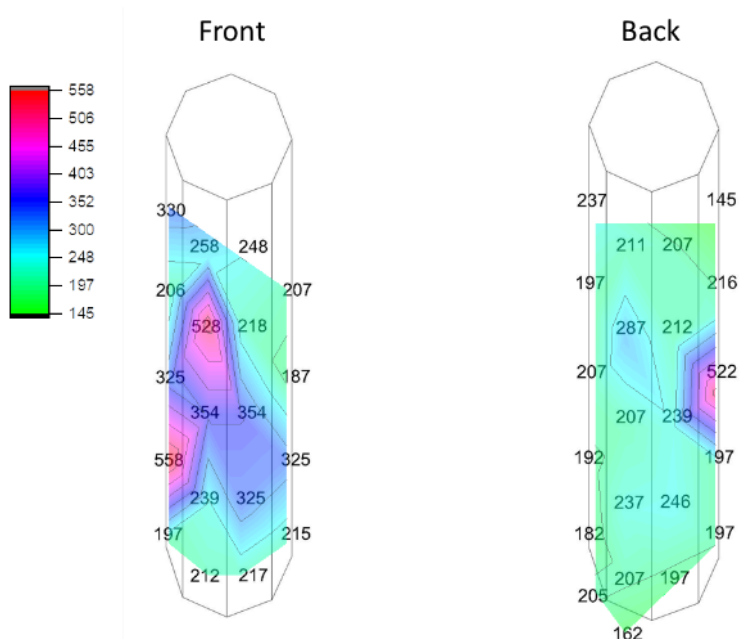

Figure 30. Colour map based on the surface humidity results with Protimeter MMS2 on the octagonal column of the Proshian family room.

In all these maps it was possible to notice discontinuities according to the position of the area under analysis and we can hypothesize that these variations are due to different materials and heterogeneity present but also to the chamber microclimate. However, it is always necessary to consider that the instrument used was not the most valuable for the case study, indeed according also to the ranges calculated by the instrument, most of the surfaces would result in being in the wet range. Yet, the colour maps indicate the current situation regarding the different walls examined.

3.4. Sponge-test method

The graphical representations, delineated as colour maps based on the outcomes derived from the sponge-test, are presented in Figures 31-36. Each of these visual representations is subsequently linked to quantitative values expressed in $g/cm^2 \cdot sec$, as stipulated by the UNI Normal 11432-2011 [2]. These numerical associations are detailed in each table paired with the corresponding map. The column (Fig. 36) was considered as a single element in alignment with the previous paragraph. The scales used in the colour maps report their maximum and the minimum value according to each zone and the values are reported in grams (calculated by the subtraction of the initial and the final weight of the sponge).

The colour maps in Figure 31 depict the western wall of the analysed room, showcasing a distinct alignment of the results with the wall's morphological features and degradation patterns. This is particularly evident on the right side of the drawing, specifically at the single arch. A comparison of these values with the degradation map of the corresponding area (Fig. 20, Chpt. 3.2.) reveals a possible correlation between the two datasets. In fact, according also to Sassoni and Franzoni [50], a deteriorated stone exhibits usually a more water intake compared to its healthy counterpart. However, it is worth noting that the area on the left side of the larger central arch, which appears to exhibit a similar degradation pattern, demonstrates contrasting values.

Figure 31. Western wall of the Proshian family room. a) Colour map based on the sponge-test measurements; b) Resulted values reported in g/cm^2 · sec.

In Figure 32, the map of the columns visible from the centre of the room and the base of the upper part of the Proshian family chamber is reported. Notably, the results exhibit a substantial homogeneity, except from the left portion of the representation, where values as high as 3,53 g (0,0021 g/cm^2 · sec) are recorded.
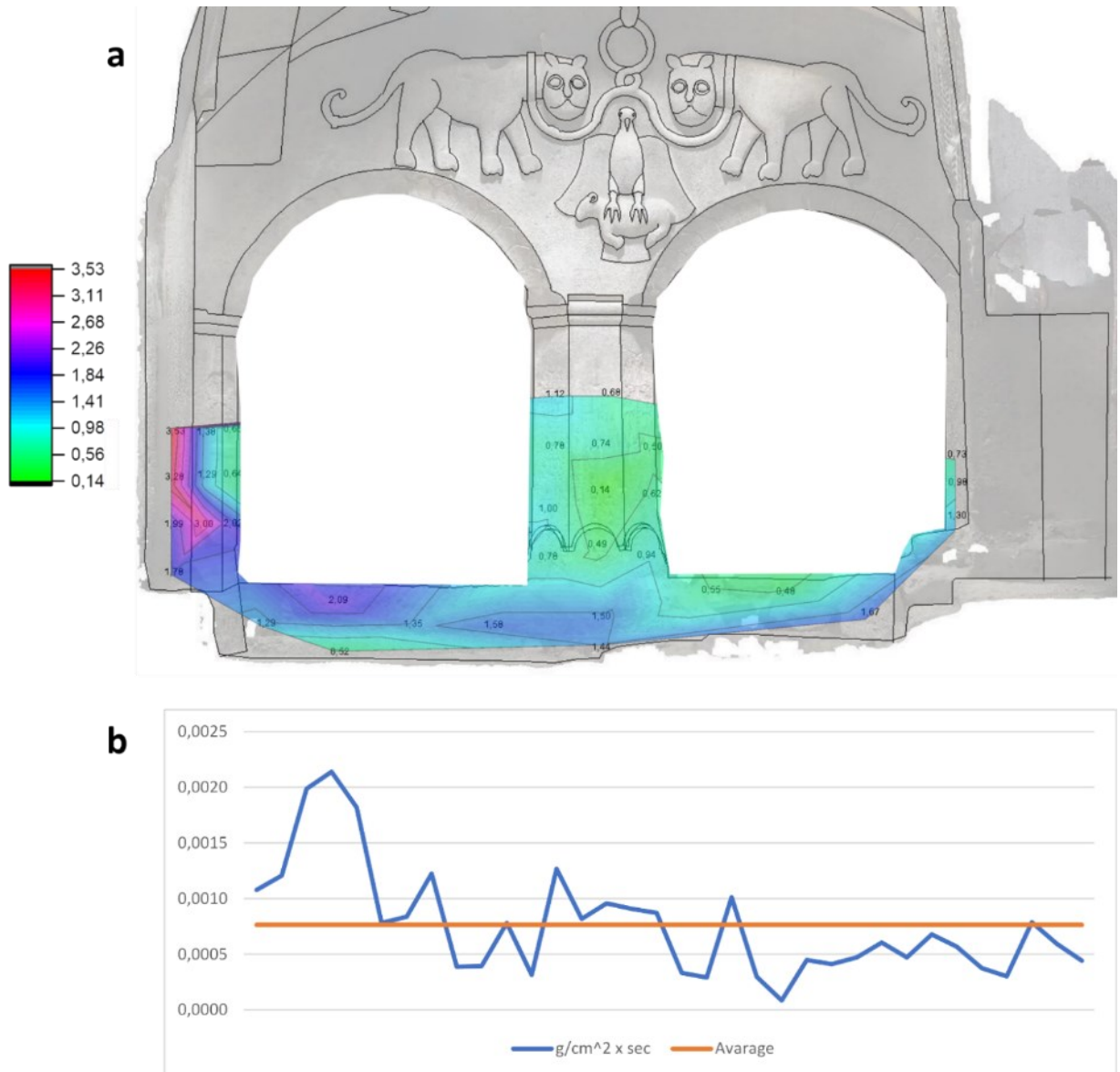
Figure 32. columns and base of the Proshian family room (view from the centre of the chamber. a) Colour map based on the sponge-test measurements; b) Resulted values reported in g/cm2 · sec.

The results of the northern wall are reported in Figure 33. The least amount of measures in this area was dictated by the homogeneity of the situation observed, which is also reflected in the corresponding degradation map (Fig. 22, Chpt. 3.2.). Consequently, the focus in this area shifted towards potential variations in accordance with elevation, although such differences were ultimately not observed. It is worth mentioning that the majority of the highest values correspond to areas with scaling.
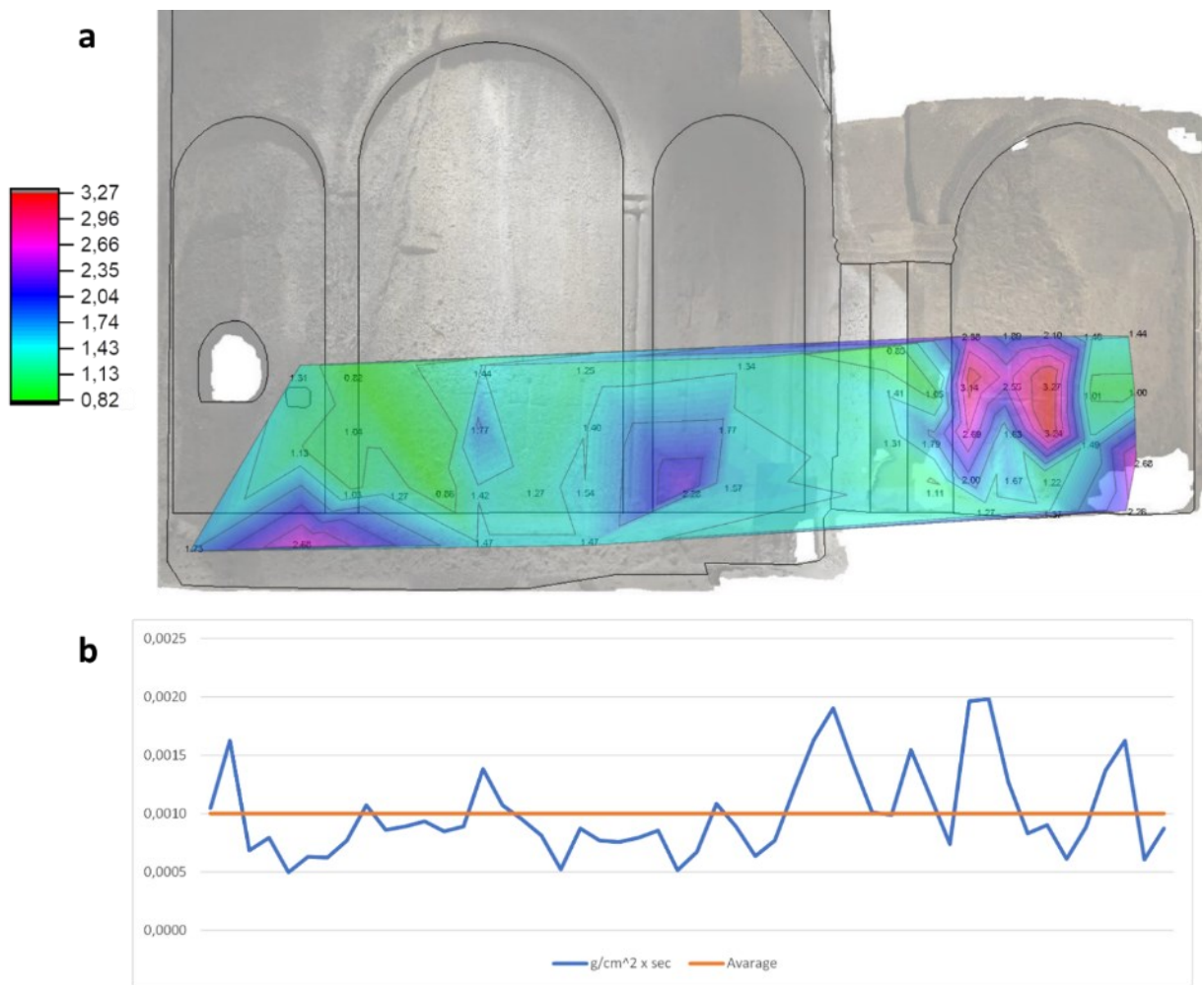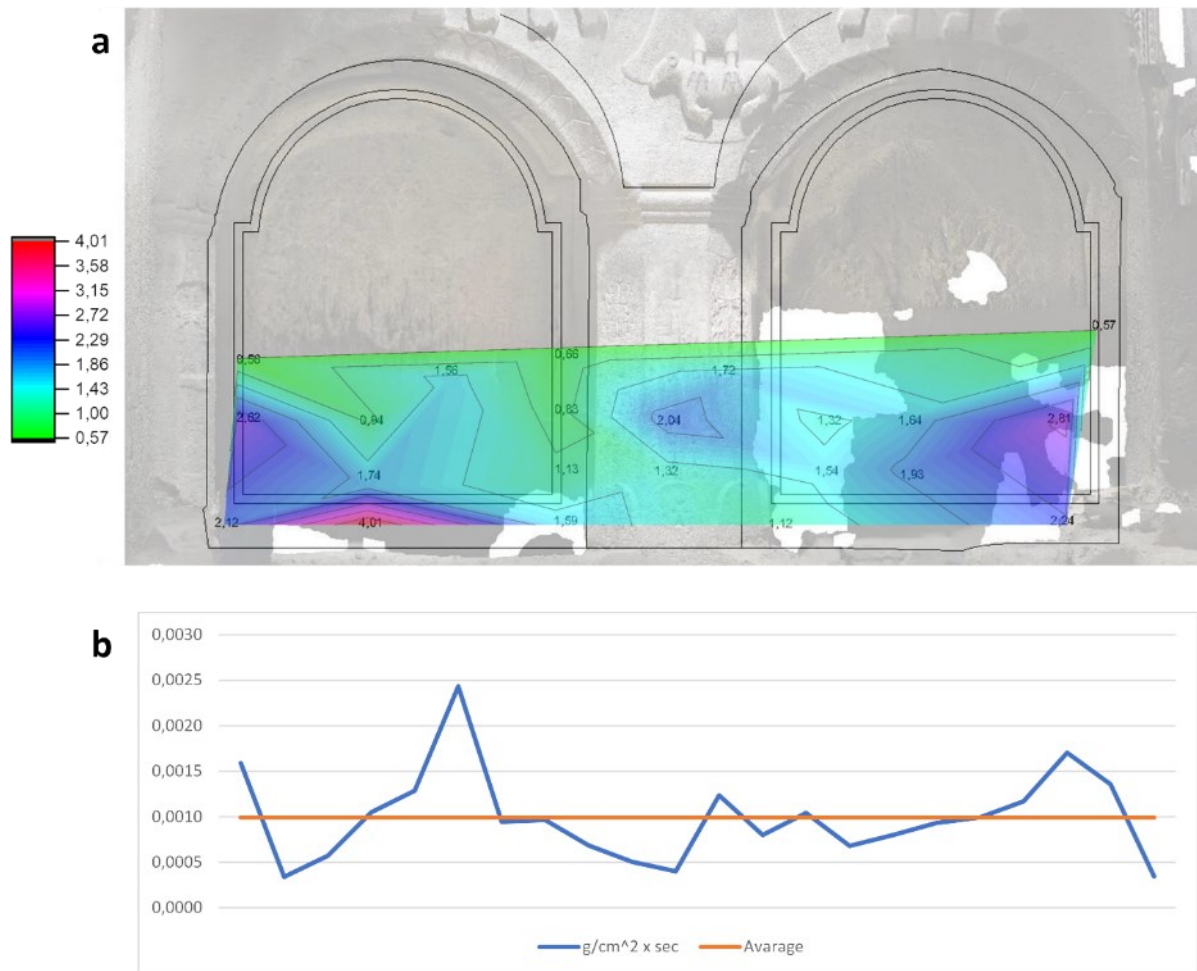
Figure 33. Northern wall of the Proshian family room. a) Colour map based on the sponge-test measurements; b) Resulted values reported in g/cm2 · sec.

The eastern part of the room (Fig. 35) exhibits values ranging from 0 g up to 3,42 g (0,0021 g/cm^2 · sec). Areas with values lower than 0,10 g are represented on the map using discrete markings to distinguish them from other zones. However, it is important to note that this limited water absorption is not indicative of a favourable condition. Instead, it is attributed to the presence of a thick layer of wax crust, which effectively renders the surface waterproof. This is one of the main problems that concerns the monastery as the presence of wax not only poses aesthetic concerns, but it can also lead to very serious mechanical issues. Stone surfaces with an extensive layer of wax or other foreign materials may be unable to naturally "breathe," leading to internal forces that can gradually weaken the structural integrity [52].

Figure 34. Eastern wall of the Proshian family room. a) Colour map based on the sponge-test measurements; b) Resulted values reported in g/cm2 · sec.

The southern wall of the room, as depicted in Figure 35, demonstrates a situation that mirrors the scaling pattern and the morphology of the room, with a minimum value of 0,14 g (0,0001 g/cm^2 · sec) and a maximum value of 2,90 g (0,0018 g/cm^2 · sec) recorded in the lower parts.
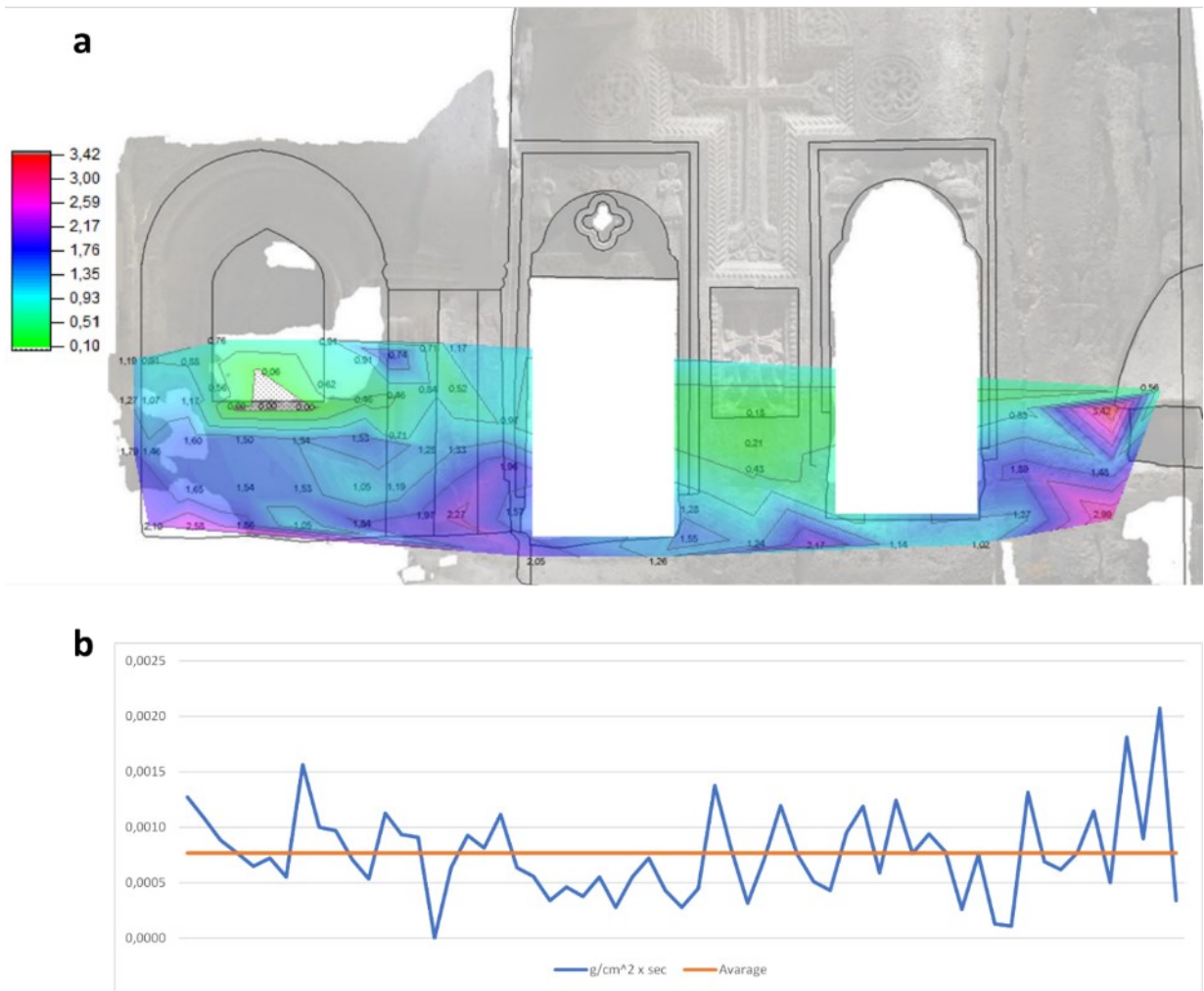
Figure 35. Southern wall of the Proshian family room. a) Colour map based on the sponge-test measurements; b) Resulted values reported in g/cm2 · sec.

Figure 36 presents the colour map of the octagonal column, with the highest value (4,72 g) observed at the base, a region subjected to degradation and seemingly composed of a distinct material compared to the main structure. In contrast, the values within the column itself exhibit remarkable uniformity, while lower water absorption values in certain points may be attributed to the presence of wax on the surface.
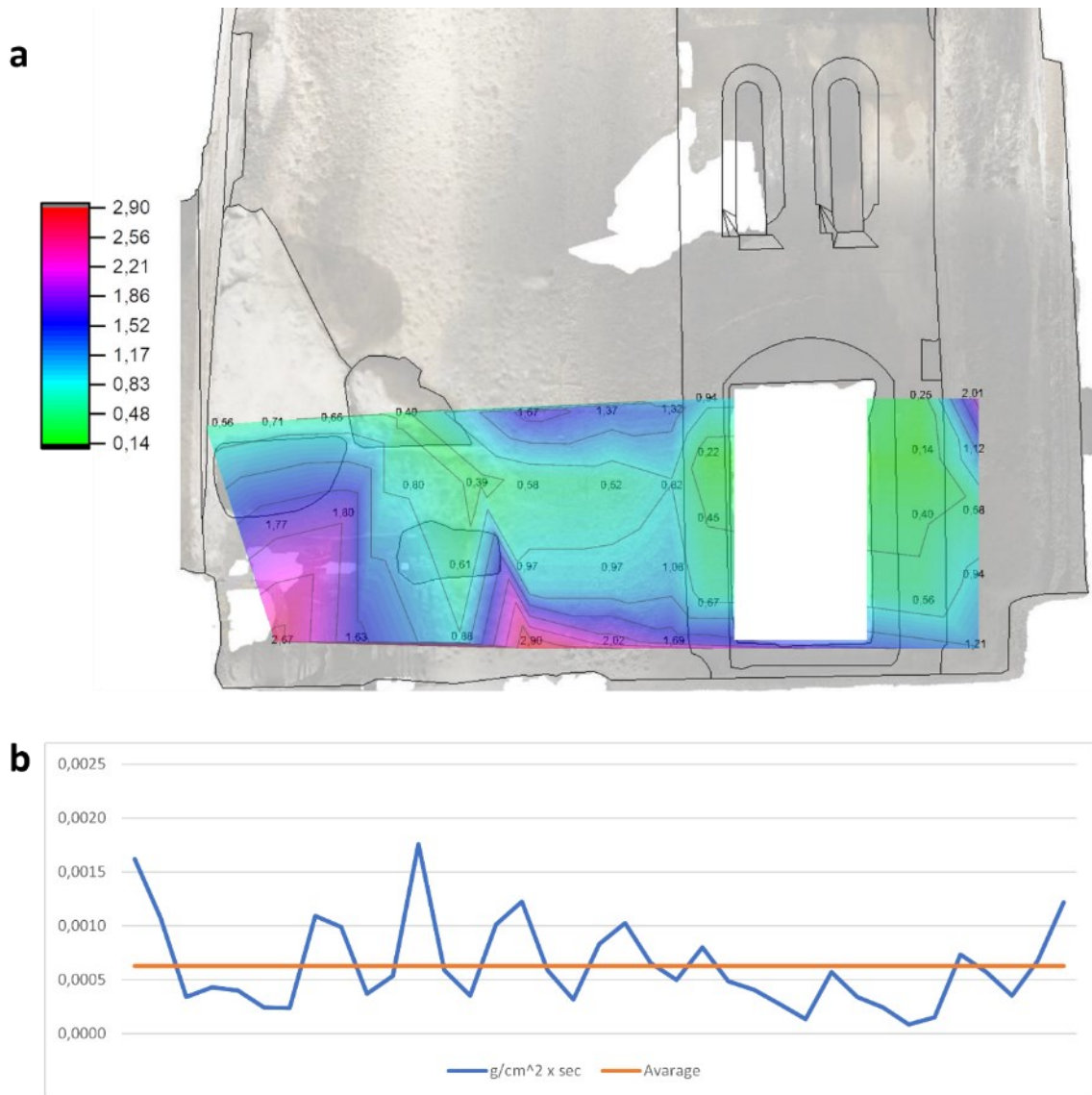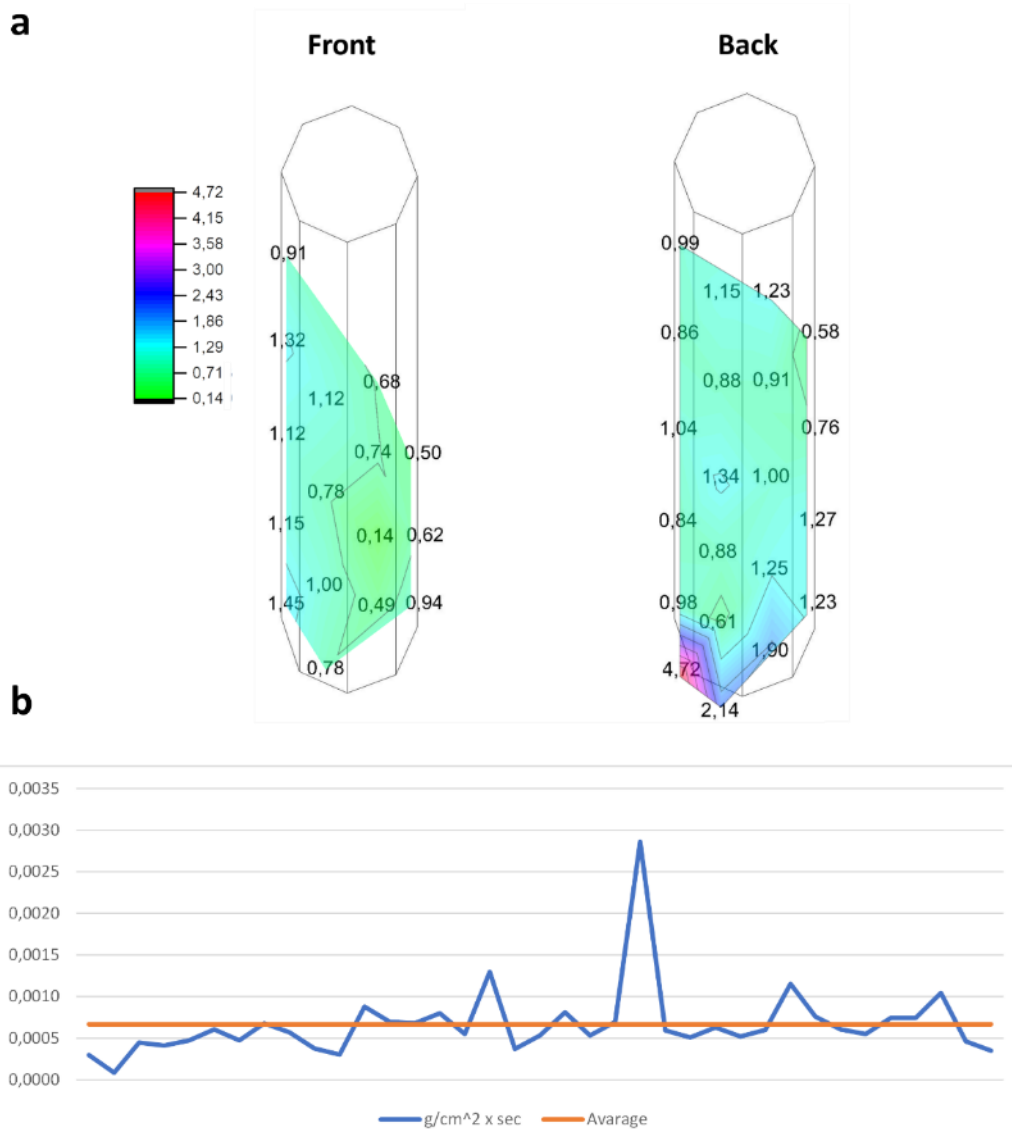
Figure 36. Octagonal column wall of the Proshian family room. a) Colour map based on the sponge-test measurements; b) Resulted values reported in g/cm2 · sec.

Throughout these findings, a recurring pattern emerges, particularly in areas exhibiting greater deterioration, where water absorption appears to increase, as seen in the scaling regions. However, when these results are compared with surface humidity measurements, discrepancies become apparent. The patterns generated by the *Protimeter MMS2* instrument do not align as closely with the degraded wall surfaces as the values obtained through the sponge-test method. Additionally, it should be noted that, considering the instrument's range of action for surface humidity, most surfaces should register as wet, resulting in negligible water absorption values, as the surfaces are already saturated. Nevertheless, it is imperative to acknowledge that these techniques operate within distinct operational ranges, with the Protimeter's range being less clearly defined due to its unsuitability for application on these types of surfaces.

3.5. Ultrasonic analysis

In this paragraph, the tomographic maps resulting from the ultrasonic analyses, are presented. These maps are accompanied by a reference scale of the time of flight which on the wall surfaces ranges from 1000 to 3000 m/s while on the column it spans from 1500 to 5000 m/s (Figg. 37-39). The survey results of the wall surfaces were also associated with the corresponding image (representative of the area) to better comprehend their localization.

Figure 38 showcases the areas we analysed on the western wall of the Proshian family room. Notably, we observe lower values (represented in black) concentrated primarily along the border of the central arch (*area b*). Conversely, higher values are evident in the region marked as "a." These findings align with the surface conditions: differential erosion on the left side of the large arch and the presence of engraved crosses on the right side. The stone between these two points exhibits lower velocity values, indicating a healthier and more compact condition.

Wedekind et al. [10] also carried out during their investigations, some ultrasonic analyses on the material that composes the Geghard rock associated with tuff. These values for the fine grain typology of tuff in dry conditions are equal to ± 2000 m/s while in the clast typology – still in dry conditions – the time of flight values correspond to ± 1500 m/s. Despite the fact that it is written nowhere that the analysed samples were effectively healthy, we can assume these values to be our references for a healthy rock, considering also the resulting values of Bris et al. [53] where Lecce stone values are evaluated. This stone, where the time of flight velocities are equal to ± 2000 m/s, is characterized by high porosity and low strength values that could be compared to the tuff variety here under analysis.

For what concerns the references for the basalt, the situation is a bit more complicated since there is no info about it in the Armenian investigations and in literature we have ultrasound velocities that span from 3000 to 4500 m/s [54, 55] according to the basalt typology. Since we do not know a lot about the basalt present in Geghard except its porosity values, we can use the Istria stone ultrasound values to have an idea of the resulting situation. In accordance with Bris et al. we know that a healthy Istria stone has values equal to ± 2700 m/s and even if these two stones are different, they have similar compactness and relatively low porosity. Istria stone is indeed often associated with porphyry [56] which as well as basalt, it is an igneous and extrusive stone [57].
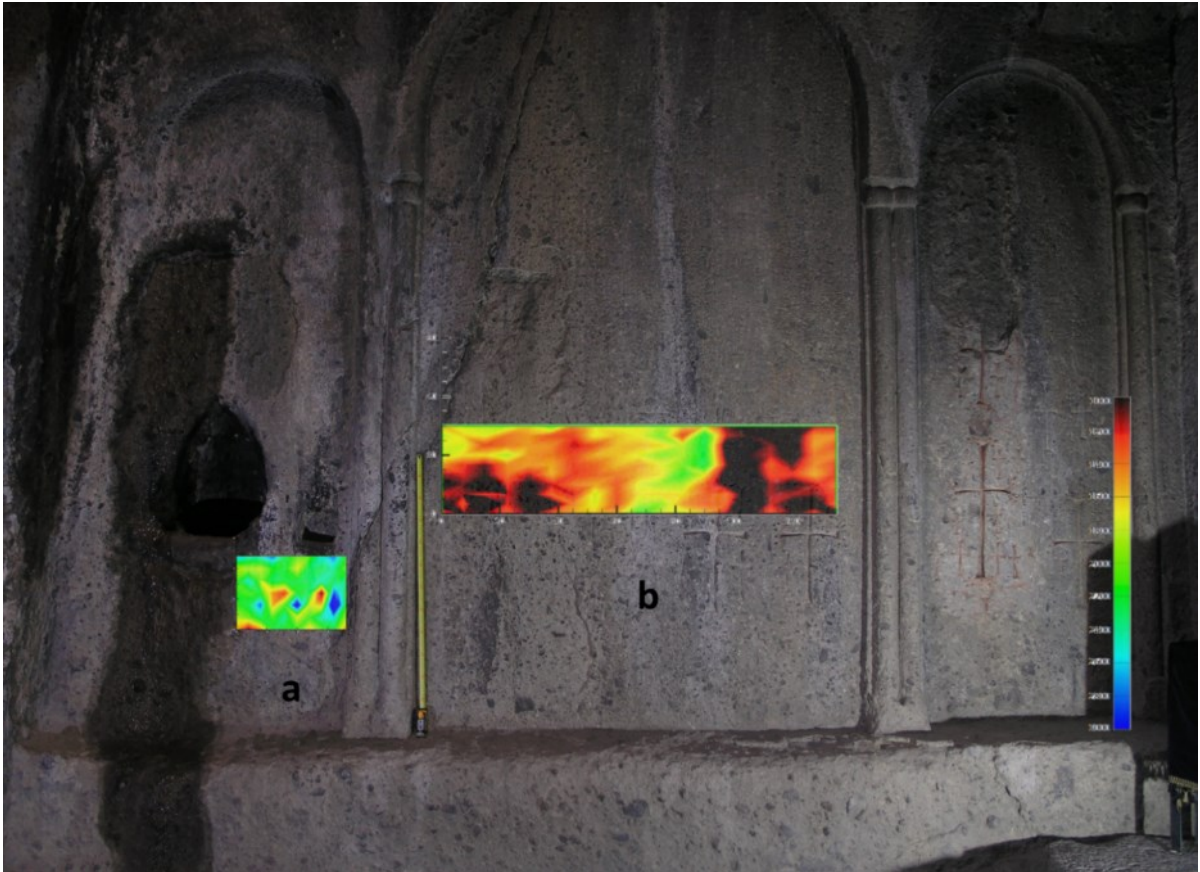
Figure 37. Tomographic results on the western wall area "a" and "b" of the Proshian family room.

For what concerns, instead, the other smaller area (*area a*) we can discern different patterns. The situation seems to be better compared to *area b* but there are localized points where lower values are still noticeable.

Moving on to *areas c* and *d* (as shown in Figure 38), we observe that *area d* predominantly reflects a compact and relatively healthy condition. However, there is a spot in the middle with slightly higher values, corresponding to an area with scaling (see the degradation map in Fig. 22, Chpt. 3.2.). In contrast, *area c* displays higher values which, confronted with the degradation map of the northern wall (Fig. 22, Chpt. 3.2.) match the degradation patterns such as scaling as well as blistering on the left side.
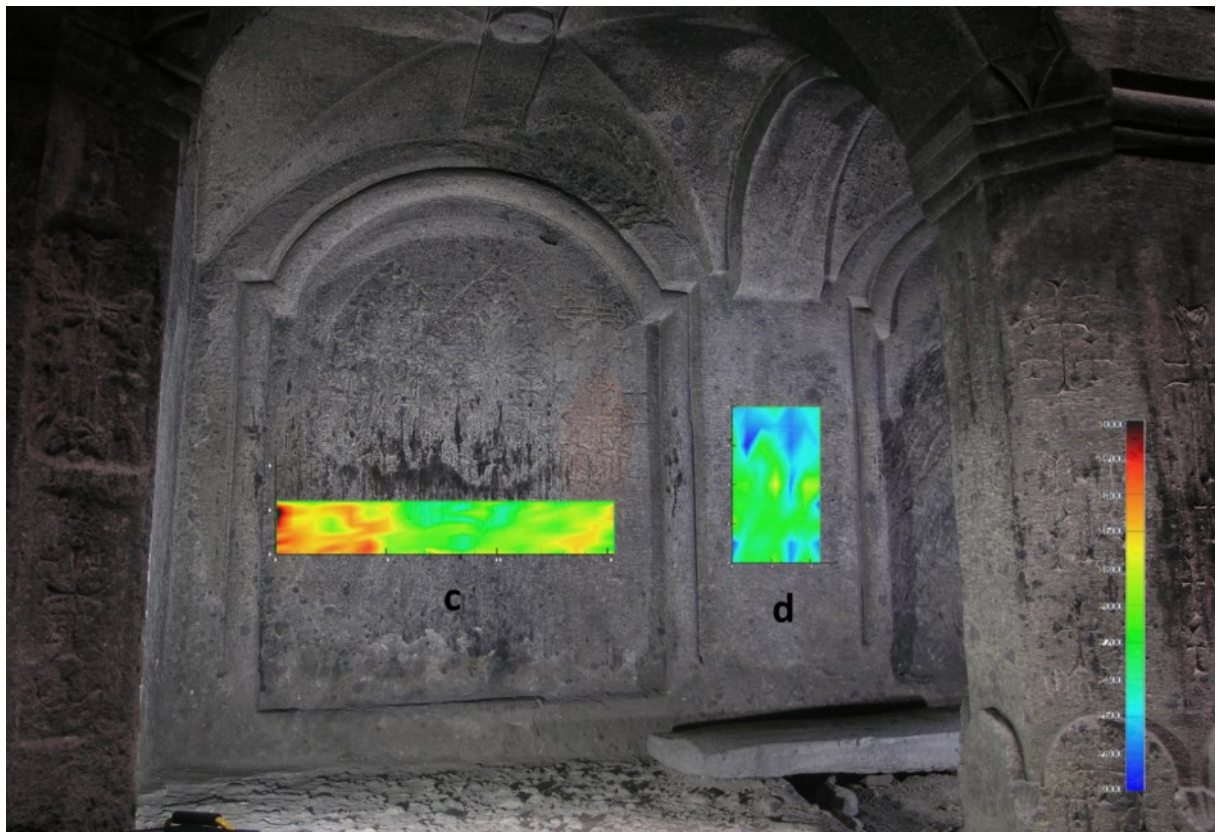
Figura 38. Tomographic results on the western wall area "c" and "d" of the Proshian family room.

The column results are reported in Figure 39. where, as previously mentioned, the scale is much higher than for the other analysed areas. This feature highlights the compactness of this architectural element reflecting what is observable to the naked eye. Anyway, Figure 39 displays different sections of the measurements where some lower values can be noticed on one edge on the upper side of the column.
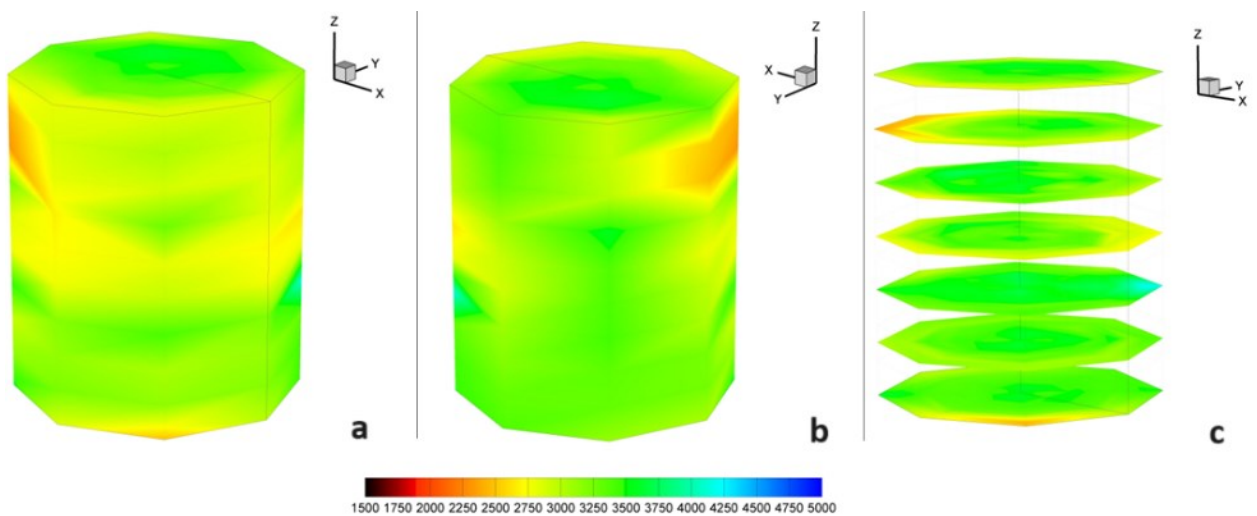
Figure 39. Tomographic results on the octagonal column of the Proshian family room.

The non-invasive techniques conducted in situ succeed in giving a general idea of the conservation condition featured in the monastery and, especially, in the room analysed. The monastery has clear problems with salt encrustations, efflorescences and black deposits. These last are probably associated with the lightening of a lot of candles every day which leads to also have lot of wax deposits that can change the original stone properties with time, making the surface waterproof and not enabling the natural breathing of the stone. The structural problems are evident, yet the comparison of the 2018 and 2023 pictures highlighted through the degradation indicators and respective linear and progressive indices demonstrate what seems to be a stable situation. However, we should consider the fact that to have a more accurate comparison of the pictures it should have been used the same kind of camera with the same light exposition and weather conditions. The humidity surface analyses carried out with the *Protimeter MSS2* are maybe those less significative: they can give an idea of the situation but the results are unpredictable and cannot be considered really trustworthy because of the impossibility of setting different materials under analysis along with the fact that moving of just a few millimetres the instrument, occasionally gave totally different results. The sponge test method, on the other hand, resulted to be one of the best techniques used. This reflects what observed with the naked eye about the degradation patterns and different morphologies present in the room. Moreover, its user-friendly application is really something important in cases such as those of the Armenian reality where often a specialised figure such as a conservation scientist is absent. Even the ultrasonic analyses gave good results coherent with what macroscopically observed but their application is much more complicated compared to the other methods used: the mobility of the instrument is much harder, and the analyses are not as much user-friendly both for the interpretation but also for how to use the instrument. In any case, it remains the most important non-invasive technique to give a quantitative picture of the stone's compactness. Finally, the degradation maps proved to be a really good means to evaluate the feasibility of the result found and to highlight the presence of discrepancies between different techniques used. In addition to this, they can give a prompt understanding of the main degradation processes that are going on and their respective localization.

3.6. Sampling campaign

The sampling campaign allowed the possibility to chemically and petrographically analyse some pieces of the Geghard monastery stones and their different degradation products. In Table 1 (Chpt. 2.6.) is reported a summary of the different laboratory investigations carried out on

each sample associated with the description of it and the macroscopic picture of where it was taken.

<u>In situ analyses</u>

3.7. Microscopic analysis

Of the 22 samples observed with the microscope, half of them are reported and commented hereinafter (Figg. 40-44). This choice was made thinking of the similarities between different specimens and some peculiarities present.

- In Figures 40-41 there are the representative microscopic pictures of the different powders collected. In Fig. 40a, sample G_14 represents the powder typology more diffused; here it is possible to notice a crystallinity aspect of a whitish/beige colour with some red crystals. In Fig. 40b we can observe the yellow powder of the sample G_17 similar to in G_8, G_10 and G_11 samples. Sample G_6 is reported in Figure 40c. This sample was taken from the red powder usually in correspondence with the carved crosses. It was also noticed that during the collection, under the red layer, a white chalky powder was present. Indeed, it seems that the presence of this colour is the result of modern graffiti. For this reason, also in the degradation maps previously observed, these features were indicated. In Figure 40d the white powder found in the upper chamber with respect to the Proshian room, is shown: this powder compared to the others really seemed to be an efflorescence due to its consistency and easy removal. The other whitish powders collected in fact, were adherent to the surfaces. Finally, in Figure 41 (sample G_7), the black powder present on most of the surfaces of the monastery, which is attributed, probably, to carbon black. The consistency of this powder was a mix of waxy and earthy texture.

- In Figure 42 two different samples are reported: G_15 (Fig. 43a and c) and G_9 (Fig. 43b, d and e). The willingness of this figure is to compare two materials that with a magnification of 6,3x (Fig. 42c and d) seem to be the same. However, G_15 is a wax deposit specimen while G_9 is a little piece of material that was found in a scaling area of the vertical surfaces of the Proshian family room. This is also clearer on the 1,6x magnification images reported (Fig. 42a and b). As proof that G_9 was actually a piece of stone material, its cross-section is also reported (Fig. 42d).

- Figure 43 reports the cross-sections of 4 different samples: G_2, G_5, G_13 and G_22. Figure 43a reports the cross-section of the bottom of G_2, a piece of what seems to be

mortar to the naked eye. In the bottom part of this specimen, a piece of the stone is embedded of which it was studied the stratigraphy. It is possible to notice how the higher part witnesses a darker and homogeneous layer, fading with depth. This behaviour can be also observed in sample G_13 (Fig. 43b) and could be possibly associated with degradation phenomena from which the entire monastery seems to suffer: the presence of carbon black due to candles. In Figure 43c and d, G_5 and G_22 are respectively reported. Here, it was interesting to observe that these pieces of stone, taken in two different areas of the monastery but thought to be a similar kind of stone once collected, were actually two totally different stones. Figure 43c is the cross-section of one little piece of the stone of the analysed room in this thesis work. This sample, more than the others, confirms the big heterogeneity already observed with previous analyses.

- Finally, in Figure 44 are reported the microscopic pictures of the cement/mortar observed on the surfaces of the monastery: Figure 44a shows a piece of the sample taken outside (G_20) while Figure 44b shows the sample of mortar took inside the room (G_2).
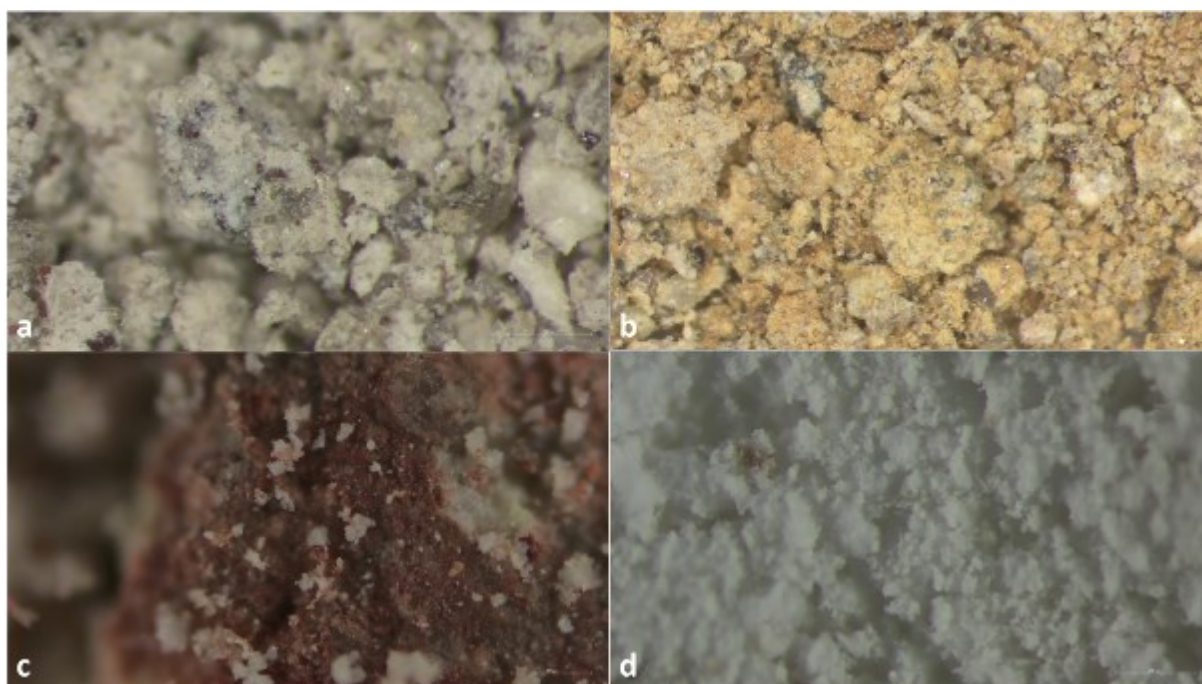
Figure 40. Miscroscopic pictures of different kind of powders present in the Geghard Monastery. a) sample G_14 6,3x; b) sample G_17 3,2x; c) sample G_6 9,45x; d) sample G_19 9,45x.

Figure 42. Microscopic picture of black powder, sample G_7 6,3x.

Figure 41. Microscopic pictures of sample G_9 and G_15. a) G_15 1,6x; b) G_9 1,6x; c) G_15 6,3x; d) G_9 6,3x; e) G_9 5x.

Figure 43. Cross sections microscopic pictures. a) G_2 1,25x ; b) G_13 1,25x ; c) G_5 1,25x ; d) G_22 1,25x.

Figure 44. Microscopic picture of sample G_2 and G_2. a) G_20 3,2x; b) G_2 1,6x.

3.8. Measurements of soluble salts

The results of the measurement of soluble salts conductivity on the selected samples, revealed unexpected relatively low values as shown in Tabl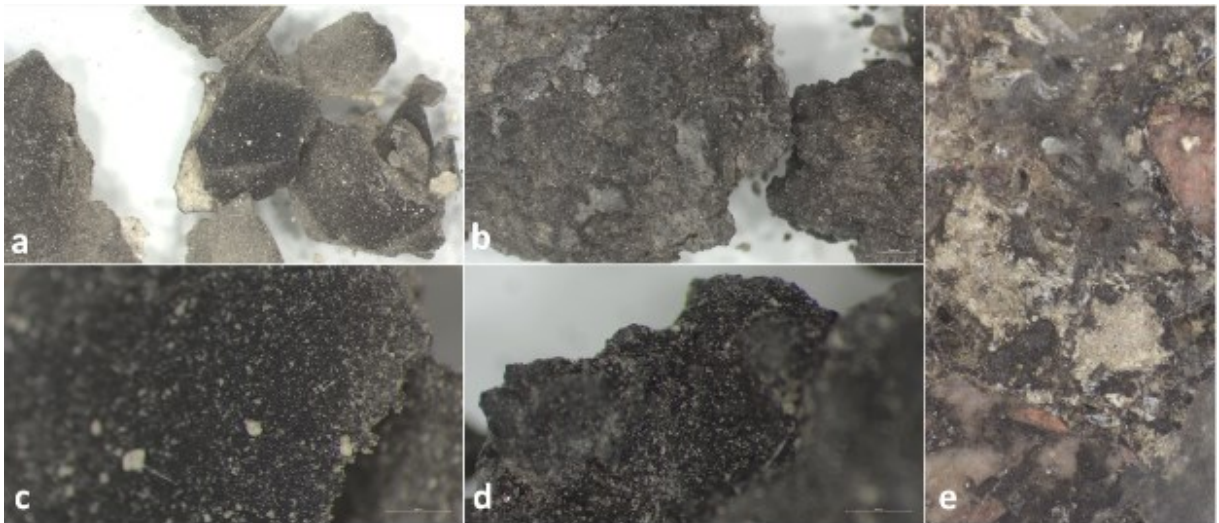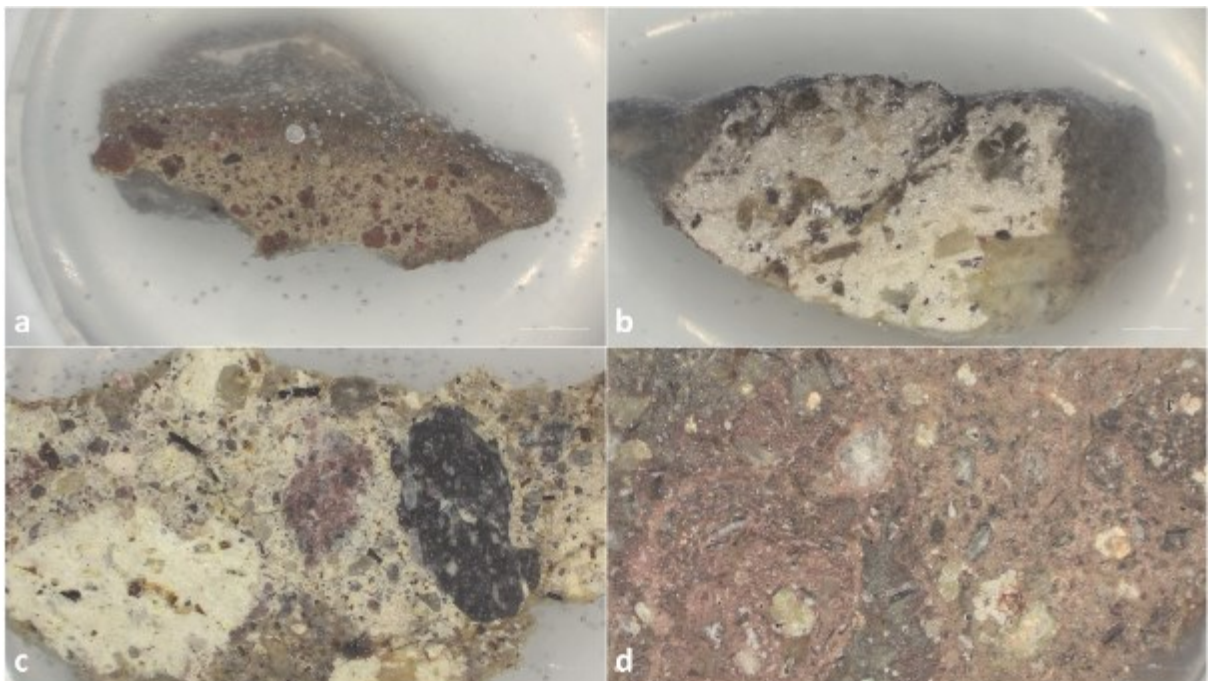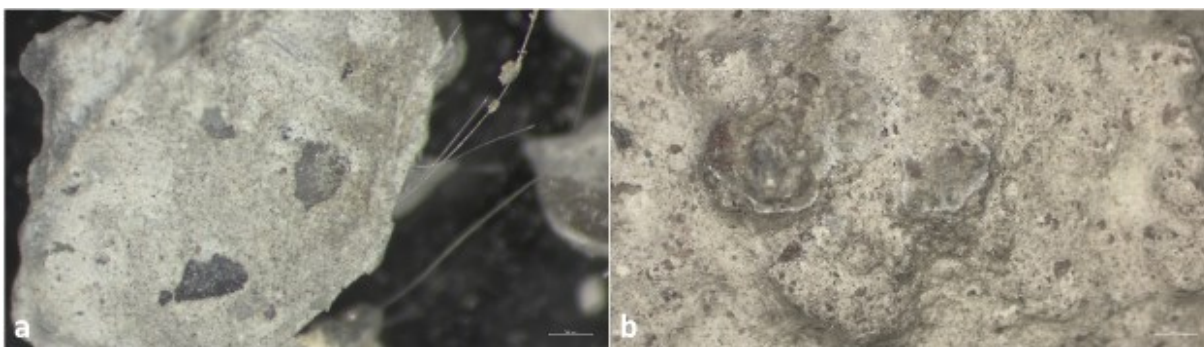e 4. In fact, sample G_16 and G_19 (described as an efflorescence) were actually selected for their visible crystalline appearance, also observed with the microscope.

Table 4. Salts conductivity results.

Sample name	salts conductivity µS/cm
G_16	39,1
G_19	56,7
G_5_int	4,27
G_5_ext	7,84

However, despite the values measured are effectively low and to have more representative results we should have had the possibility to analyse a bigger number of specimens, these values can be considered proportionally coherent. Among the 22 samples collected, G_19 was the only one taken from the most evident salt efflorescence. In fact, in this table, this specimen is also the one that shows the higher salt conductivity followed by G_16. Also, G_5 shows a slight difference between the external and the internal part possibly attributed to the salt encrustation present on the surfaces of the whole monastery.

3.9. Fourier Transform Infra-Red (FTIR) spectroscopy

The general results of the FTIR analyses performed are reported in Table 5 and from Figures 45-48 also some representative spectra are shown. The question marks in the table are used to indicate the hypothesized mineral according also to the outcomes given by the XRD.

In the majority of the resulting investigations, the infrared spectra exhibit the characteristic absorption of silicate minerals (1100-1000 cm^{-1}), the O–H stretching and bending vibrations at 3400, 3530, and at 1620 cm^{-1} and sometimes also those of calcite (peaks between 1400-1430 cm^{-1}, 875 and 715 cm^{-1}) [38].

Table 5. Results of the FTIR investigations.

Sample name	FTIR results
G_1	Silicate minerals (Anorthite? & Quartz?)
G_2	Gypsum; Calcite; Silicate minerals (Anorthite? & Quartz?)
G_3	Gypsum; Calcite?; Silicate minerals (Anorthite? & Quartz?)
G_3 salt extraction	Gypsum; Silcate mineral - traces (Anorthite?); Nitrates (Ca(NO3)2 ?)
G_4	Gypsum; Calcite?; Silicate minerals (Anorthite? & Quartz?)
G_6	Gypsum; Silicate minerals (Anorthite? & Quartz?)
G_7	Organic fraction; Silicate minerals (Anorthite? & Quartz?); Calcite?
G_8	Gypsum; Silicate minerals (Anorthite? & Quartz?)
G_9	Organic fraction; Calcite? Silicate minerals (Anorthite? & Quartz?)
G_10	Silicate minerals (Anorthite? & Quartz?)
G_11	Gypsum; Silicate minerals (Anorthite? & Quartz?)
G_11 **(KBr)**	Gypsum; Silicate minerals (Anorthite? & Quartz?); Organic fraction; Nitrates (Ca(NO3)2?)
G_12	Gypsum; Silicate minerals (Anorthite? & Quartz?)
G_13_surface	Gypsum; Silicate minerals (Anorthite? & Quartz?)
G_13_interior	Gypsum; Silicate minerals (Anorthite? & Quartz?)
G_14	Gypsum; Silicate minerals (Anorthite? & Quartz?)
G_16	Gypsum; Silicate minerals (Anorthite? & Quartz?)
G_17	Gypsum; Silicate minerals (Anorthite? & Quartz?)
G_18	Organic fraction; Silicate minerals (Anorthite? & Quartz?)
G_19	Calcite; Sodium carbonate?

The G_13 spectrum (Fig. 45a) shows the main peaks observable in most of the analysed samples (i.e. silicate minerals and gypsum). Silicate minerals were not easy to distinguish by the FTIR investigations though the one that repeats in each sample (between 1000–1015 cm^{-1}) is hypothesized to be anorthite according to the XRD results as well as the quartz peaks. In Figure 45b is reported instead the sample G_9 which always shows the peaks associated with anorthite and quartz but also the characteristic peaks of an organic fraction around 2900-2800 cm^{-1}. Moreover, a peak associated to calcite is also observed (719 cm^{-1}).
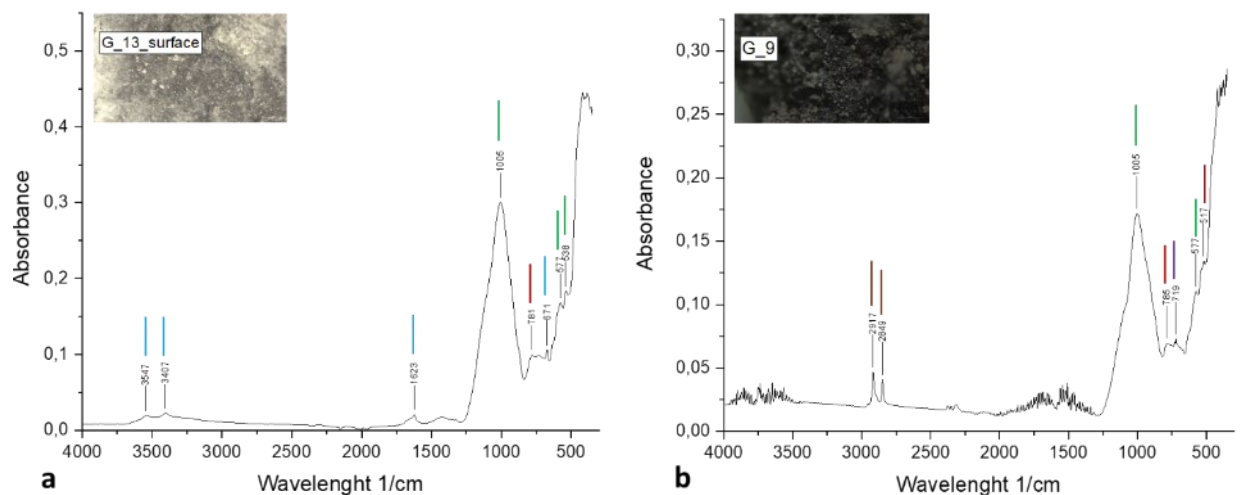
Figure 45. ATR-FTIR spectra of sample G_13 and G_9. a) sample G_13 shows the presence of gypsum (3547-3407-1623-671 cm⁻¹), and silicate minerals (anorthite? 1005-577-538 cm⁻¹ and quartz? 781 cm⁻¹); b) Sample G_9 shows peaks associated with organic fraction (2917-2849 cm⁻¹), silicate minerals (anorthite? 1005-577 cm⁻¹ and quartz? 785-517 cm⁻¹) and calcite (719 cm⁻¹).

In Figure 46, the spectra outcomes of G_11 are shown: in Figure 46a the ATR-FTIR resulting spectrum and in Figure 46b the one made with a KBr pellet that allowed the more accurate identification of the different peaks revealing also those associated to the nitrate group (1384 cm⁻¹) and to the organic fraction (2923–2851 cm⁻¹). The gypsum peaks, on the other hand are much more highlighted and thus easier to be confirmed.
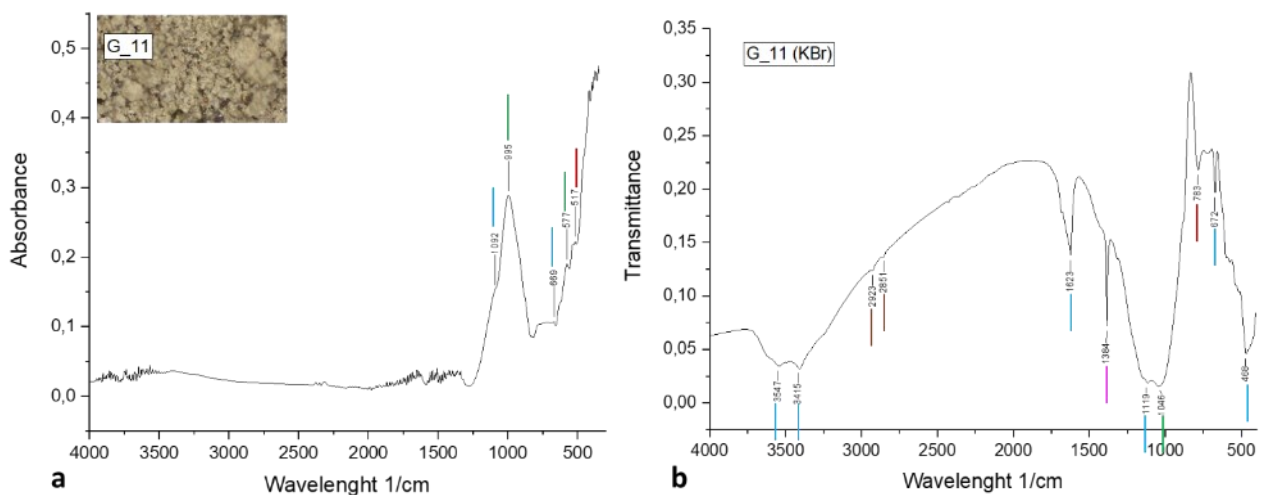
Figure 46. FTIR spectra of sample G_11. a) ATR-FTIR results show the presence of gypsum (1082-669 cm⁻¹), and silicate minerals (anorthite? 995-577 cm⁻¹ and quartz? 517 cm⁻¹); b) KBr FTIR results confirm the presence of gypsum (3547-3415-1623-1119-672-468 cm⁻¹), organic fraction (2923-2851 cm⁻¹), nitrates (Ca(NO)₃)₂? (1384 cm⁻¹), and silicate minrals (anorthite? 1046 cm⁻¹ and quartz? 783 cm⁻¹).

Sample G_2 and G_19 are respectively reported in Figure 47a and 47b because of their differences observed compared to the other samples. Both samples show peaks associated with calcium carbonate (calcite) but while G_2 also got the peaks associated with the silicate minerals and gypsum like most of the other specimens, G_19 shows just the peaks of calcite

and those attributed, most likely, to sodium carbonate (1083 and 700 cm^{-1}). In fact, G_19 is the sample collected from the upper chamber (with respect to the Proshian family room) which showed the typical morphology and consistency of an efflorescence. The presence of sodium carbonate could be referred to the use of hydraulic mortars in previous restoration work, or to the application of a silica-based consolidant [58]. Unfortunately, not much information on past interventions is available.
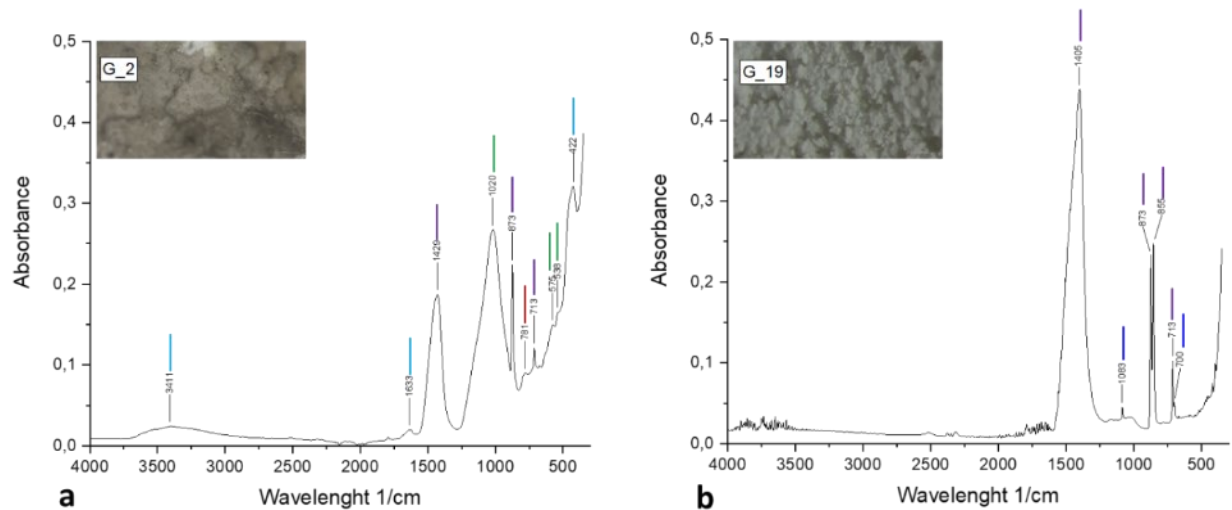

Figure 47. ATR-FTIR spectra of sample G_2 and G_19. a) G_2 shows the presence of gypsum (3411-1633-422 cm^{-1}), calcite (1429-873-713 cm^{-1}) and silicate minerals (anorthite? 1020-575-538 cm^{-1} and quartz? 781 cm^{-1}); b) G_19 shows the presence of calcite (1045-873-855 cm^{-1}) and sodium carbonate? (1083-700 cm^{-1}).

Finally, sample G_3 with its respective salt extraction is reported in Figure 48a,b. Both spectra show the presence of gypsum but in the one relative to the salt extraction, also peaks typical of the nitrate group at 1345, 1083 and 826 cm^{-1}. The peak at 1005 cm^{-1} is probably due to the solid fraction that remained after the extraction.
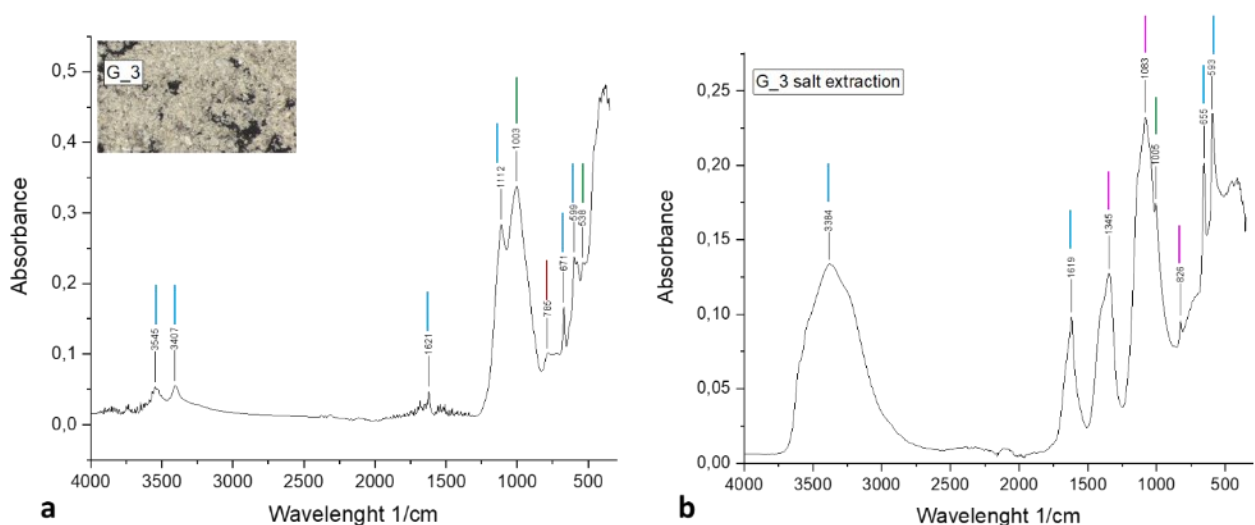
Figure 48. ATR-FTIR spectra of sample G_3 and its salt extraction. a) G_3 shows the presence of gypsum (3545-3407-1621-1112-671-599 cm^{-1}), and silicate minerals (anorthite? 1003-538 cm^{-1} and quartz? 785 cm^{-1}); b) The salt extraction of G_3 confirms the presence of gypsum (3384-1619-655-593 cm^{-1}), nitrates (Ca(NO)$_3$)$_2$? (1345-1083-826 cm^{-1}) also the remaining peaks correspondent probably to silicate minerals (anorthite? 1005 cm^{-1}) is visible.

3.10. Raman spectroscopy

The G_13 and G_21 out coming Raman spectra are shown in Figure 49. In both samples peaks associated with silicate species are found (between 400 and 600 cm^{-1}). In sample G_21 (Fig. 49b) the peaks within the green area are probably to be associated with a biological patina suggested also by the macroscopic and microscopic observations. G_13 instead show a peak attributed to calcite around 1080 cm^{-1} and the peaks at 1616 and 2918 cm^{-1} could be the results of the presence of carbon black. The presence of these species would be coherent with what was hypothesized: silicate minerals were also found with FTIR spectroscopy and with XRD which suggested the presence of anorthite; the presence of carbon black was alleged on the basis of the in situ visual survey. In fact, lot of candles are lit daily in the monastery and this, with time, can create problems as we also noticed through the degradation maps and confirmed by the cross-sections observed with the microscope.
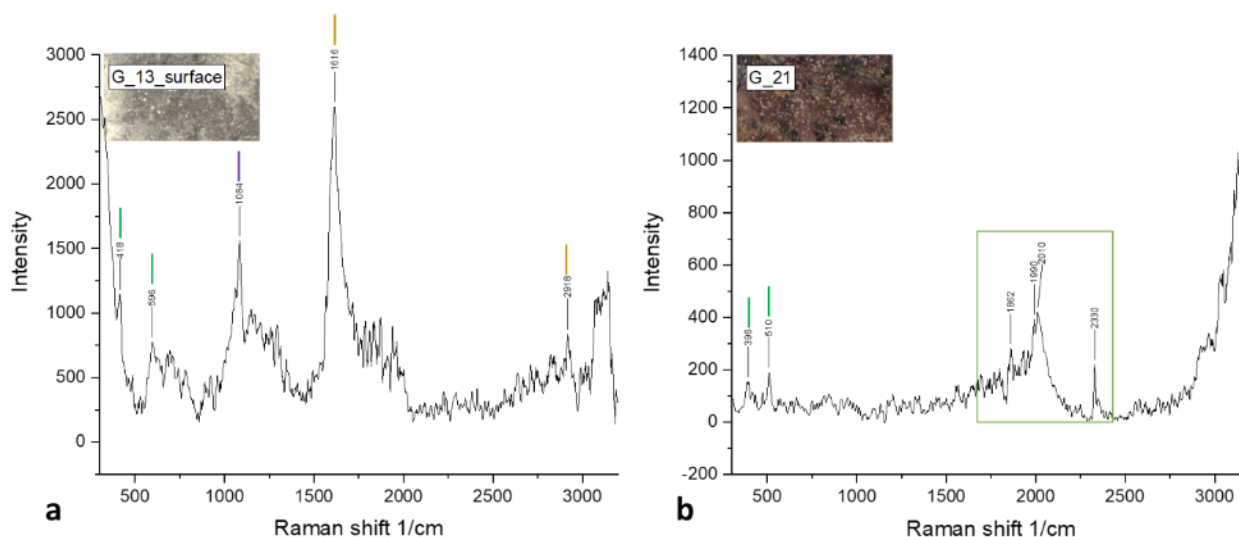
Figure 49. Raman spectra of G_13 and G_21. a) G_13 shows the presence of carbon black (1616- 2918 cm^{-1}), calcite (1084 cm^{-1}), and silicate minerals (anorthite? 418-595 cm^{-1}); b) G_21 shows biological patina peaks? (1662-1990-2010-2330 cm^{-1}), and silicate minerals (anorthite? 396-510 cm^{-1}).

3.11. X-Ray Diffraction

The 2 diffraction patterns obtained from sample G_5 (Fig. 50a,b) show a lot of peaks attributed to more than one mineralogical species overlapping. To distinguish between the powders analysed, we have labelled one as "darker" (Figure 50a) and the other as "whiter" (Figure 50b). Moreover, while some peaks are shared between the two powders, the whiter one, in particular, presents significant overlapping peaks, potentially affecting the result precision. The XRD of the darker powder show the presence of anorthite (80,4 %) followed by biotite (6,2 %). In contrast, the whiter powder displays a balance between anorthite (65,9%) and phlogopite (21 %). This latter mineral was the sole mineralogical species capable of matching the peak at 8°,

as determined by the *MATCH! Phase Analysis using the Powder Diffraction* library embedded in the software, thus it was specifically selected for this purpose.

However, even if these findings have contributed to a clearer understanding of the composition of one of the main stones in the Geghard complex and aided in the interpretation of spectroscopic investigations, it is advisable to complement these results with a mineralogical analysis on thin sections to provide further confirmation of our findings.
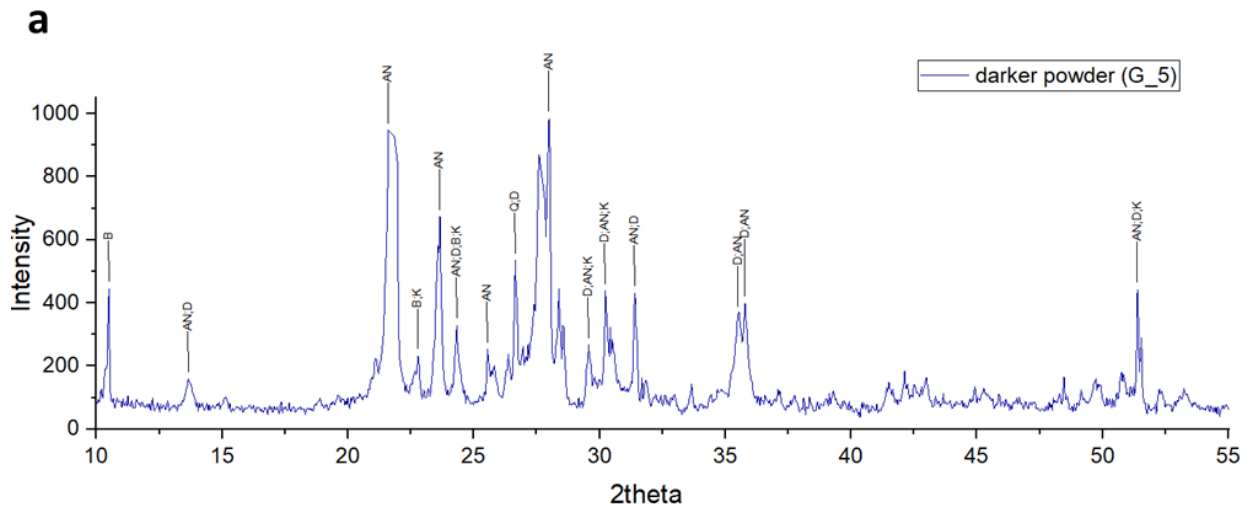
AN: Anorthite (80,4%); B: Biotite (6,2%); K: Kaersutite (4,6%); Q: Quartz (4,6%); D: Diopside (4,1%).
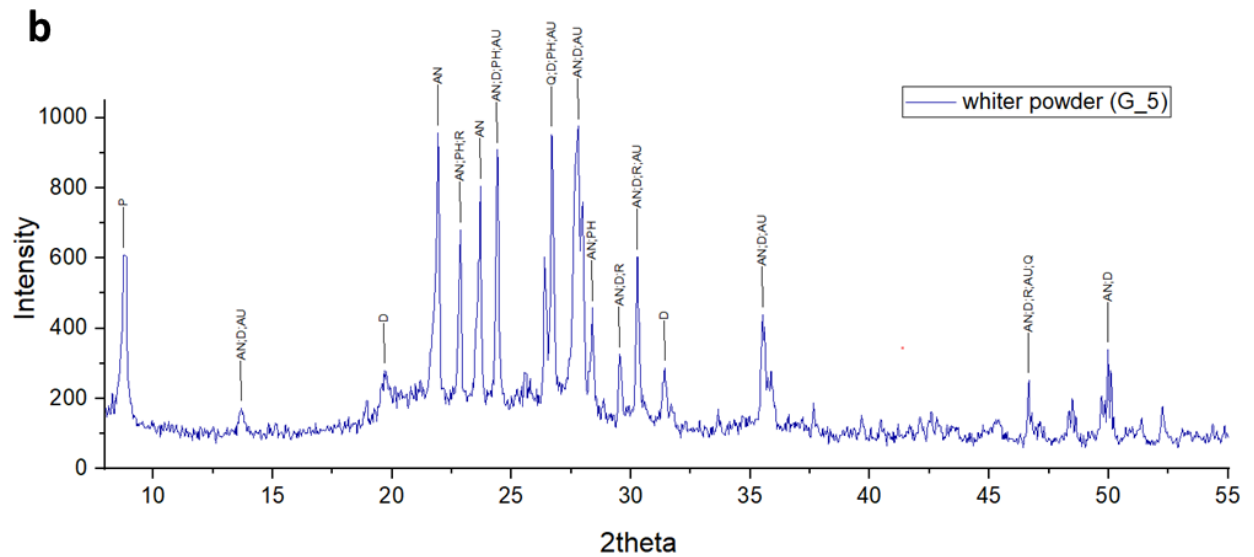
AN: Anorthite (65,9%); PH: Phlogopite (21%); Q: Quartz (8,1%); AU: Augite (2,5%); R: Richterite (1,4%); D: Diopside (1,1%).

Figure 50. XRD results of sample G_5. a) darker powder of G_5; b) whiter powder of G_5.

[50] Camuffo D. Il riscaldamento nelle chiese e la conservazione dei beni culturali: guida all'analisi dei pro e dei contro dei vari sistemi di riscaldamento. Electa; 2007

[51] Sassoni E., Franzoni E. Influence of porosity on artificial deterioration of marble and limestone by heating. In: Applied Physics A. 2013

[52] greenspec.co.uk (Internet). The importance of breathability in old buildings, greenspec (accessed in September 2023). Available at: https://www.greenspec.co.uk/building-design/importance-of-breathability-in-old-buildings/

[53] Bris T., Delegou E., Morabito M., Zendri E., Moropoulou A. High temperatures impact on the durability of natural stones: An assessment by means of ultrasound pulse velocity measurements. In: Advanced Nondestructive and Structural Techniques for Diagnosis, Redesign and Health Monitoring for the Preservation of Cultural Heritage. 2022

[54] Sekine T., Kobayashi T., Nishio M., Takahashi E. Shock equation of state of basalt. In: Earth Planets Space. 2008

[55] Stanchits S., Vinciguerra S., Dresen G., Ultrasonic Velocities, Acoustic Emission Characteristics and Crack Damage of Basalt and Granite. In: Pure and Applied Geophysics. 2006

[56] biblio.toscana.it (Internet). Pietra d'Istria, Biblio Toscana (accessed in September 2023). Available at: https://biblio.toscana.it/argomento/Pietra%20d'Istria

[57] Klein C. *MINERALOGIA*. Prima edizione, Zanichelli. 2015 (2004).

[58] Kraus K., Droll K. INVESTIGATIONS OF SOLUBLE SALT CONTENTS IN MODERN HYDRAULIC LIME MORTARS - TEST METHOD AND FIRST RESULTS. In: International RILEM Workshop on Repair Mortars for Historic Masonry. 2005

4. Conclusions

In conclusion, this work thesis accomplishes to give guidelines for future interventions in the Geghard monastery that could also be applied in other Armenian realities as well as other secluded heritages with similar situations. Specifically, most of the conducted in situ investigations are user-friendly thanks to their easy application. However, a digital transposition of the results especially associated with colour maps is truly important since it can give an immediate and simple understanding of the studied circumstances.

The non-invasive in situ analyses carried out gave also important indications of the state of conservation of the monastery, primarily of the room analysed. The first step was the visual survey with the development of degradation maps which allow us to quickly realize the localization and main ongoing degradation phenomena. This was useful also for the comparison of the other non-invasive analyses. The comparison of the Geghard status over 5 years thanks to the use of 2018 pictures, emphasized quite the stability of the structure even though from a first look, it seems that is in a very and urgent precarious situation.

However, the relationship between water and materials, studied with the sponge-test method on the *Žamatoun* surfaces, highlighted a great heterogeneity and a close connection with the degradation patterns present: in correspondence of wax deposit there is less o no absorption of water due to the impermeability properties of this deposit and in scaling areas, a bigger absorption of water is noticed.

The parallel between calculated values and room heterogeneities was observed also with the ultrasonic measurements. Hither can be observed a difference among different analysed zones, in particular between wall areas and the big octagonal column but also according to the degradation patterns present along with surface unevenness.

The instrument used for the surface humidity measurements emerged to give not really significative values most likely due to the impossibility of setting the right analysed material. Anyway, if in future these results were compared with new ones taken with a more appropriate instrument, the current colour maps could be combined.

Additionally, laboratory analyses in general – where they are possible to carry out – are important for the completeness of a survey since they can support or disprove the hypotheses after the preliminary and non-invasive measurements. Thanks to the sampling campaign in Geghard, microscopic observations, salt conductivity measurements, FTIR, Raman and XRD were possible to manage. Microscopic observations are always suggested to be carried out to

eventually notice some peculiarities not observable to the naked eye. In the Geghard case, particularly the cross-sections made it possible to observe the stratigraphy linked to degradation. Moreover, despite the fact that salt conductivity measurements gave not-so-high values, FTIR spectroscopy especially confirmed the presence of these species divided essentially into sulphates and nitrates that respectively could be gypsum and calcium nitrate. The silicate groups present in almost all the samples were also confirmed by the XRD measurements. Finally, Raman spectroscopy acknowledges the presence of carbon black, possibly strictly related to the everyday lightening of candles. These, with time, create not just aesthetic issues due to the colour change of the surfaces and wax deposit but their combustion tends to impermeabilize the surface too creating problems with the original capacity of the stone to breathe. For this reason, the restoration interventions proposed by the Armenian restorer Mery Danielyan (mentioned in the introduction chapter 1.2.5.) could be not the solution to solve the problems linked to water. The willingness to render all the surfaces waterproof could seem a good solution at the beginning but the application of extraneous materials on surfaces has often created problems over time.

Comprehensive bibliography

Ahmad A., Pamplona M., Simon S. Ultrasonic testing for the investigation and characterizatio of stone – a non-destructive and transportable tool. In: Studies in Conservation. 2014

Alzboon K. K., Al Smadi B. M., Al-Khawaldh S. Natural Volcanic Tuff-Based Geopolymer for Zn Removal: Adsorption Isotherm, Kinetic, and Thermodynamic Study. In: Water Air and Soil Pollution. 2016

Arzumanyan A. A., Arzumanyan A. A., Qaramyan H. H., Muradyan N. G. CONCEPTUAL APPROACHES TO SOLVING THE ISSUE OF REINFORCING THE ROCK - CUT STRUCTURES OF GEGHARD MONASTERY COMPLEX. In: Architectural and Engineering Research; 2021

Aslanian A. La struttura geologica della zona di G(h)eghard. In: Documenti di Architettura Armena | G(h)eghard. Edizioni Ares; 1973

Bris T., Delegou E., Morabito M., Zendri E., Moropoulou A. High temperatures impact on the durability of natural stones: An assessment by means of ultrasound pulse velocity measurements. In: Advanced Nondestructive and Structural Techniques for Diagnosis, Redesign and Health Monitoring for the Preservation of Cultural Heritage. 2022

Brunetti B., Miliani C., Rosi F., Doherty B., Monico L., Romani A., Sgamellotti A. Non-invasive Investigations of Paintings by Portable Instrumentation: The MOLAB Experience. In: Springer, Analytical Chemistry for Cultural Heritage. Mazzeo R.; 2016

Camuffo D. Il riscaldamento nelle chiese e la conservazione dei beni culturali: guida all'analisi dei pro e dei contro dei vari sistemi di riscaldamento. Electa; 2007

Camuffo D., MICROCLIMATE FOR CULTURAL HERITAGE Measurement, Risk Assessment, Conservation, Restoration, and Maintenance of Indoor and Outdoor Monuments. Third edition. Elsevier; 2019

Casadio F., Daher C., Bellot-Gurlet L. Raman Spectroscopy of cultural heritage Materials: Overview of Applications and New Frontiers in Instrumentation, Sampling Modalities, and Data Processing. Springer, Analytical Chemisty for Cultural Heritage. Mazzeo R.;2016

Chen X., Zhang Y., Hui, D., Chen M., Wu Z. Study of melting properties of basalt based on their mineral components. In: Composites Part B: Engineering. 2017

Coccato A., Jehlicka J., Moens L., Vandenabeel P. Raman spectroscopy for the investigation of carbon-based black pigments. In: Raman Spectroscopy. Wiley & Sons, Ltd; 2015

Danielyan M. RESTORATION OF HISTORICAL AND ARCHITECTURAL MONUMENTS IN ARMENIA Reconstruction and restoration of Geghardavank. In: Armenien. Kultur Natur Menschen. Mitteldeutscher Verlag; 2022

De Campos P., Appoloni C., Rizzutto M. A., Leite A. R., Assis R. F., dos Santos H. C., Silva T., Rodrigues C. L., Tabacniks M. H., Added N. A low-cost portable system for elemental mapping by XRF aiming in situ analyses. In: Applied Radiation and Isotopes. Elsevier; 2019

Fais S., Cuccuru F., Ligas P., Casula G. Integrated ultrasonic, laser scanning and petrographical characterisation of carbonate building materials on an architectural structure of a historic building. In: Bulletin of Engineering Geology and the Environment. Springer Nature; 2015

Fitzner B, Heinrichs K, La Bouchardiere D. Damage index for stone monuments. In: Protection and Conservation of the Cultural Heritage of The Mediterranean Cities. 2002

Germinario L., Oguchi C. T. Underground salt weathering of heritage stone: lithological and environmental constraints on the formation of sulfate efflorescences and crusts. In: Journal of Cultural Heritage. Science direct; 2021

Glavcheva Z. I., Yancheva D. Y., Kancheva Y. K., Velcheva E. A., Stamboliyska. B. A. Development of FTIR spectra database of reference art and archaeological materials. In: Bulgarian Chemical Communications. 2014

Gunasekaran S., Anbalagan G., Pand S. Raman and infrared spectra of carbonates of calcite structure. In: Raman Spectroscopy. Wiley & Sons, Ltd; 2006

ICOMOS-ISCS. Illustrated glossary on stone deterioration patterns. 2008.

Janek,M., Bugár I., Lorenc D., Szöcs V., Velič D., Chorvát D. Terahertz Time-Domain Spectroscopy of Selected Layered Silicates. In: Clays and Clay Minerals. 2009

Klein C. *MINERALOGIA.* Prima edizione, Zanichelli. 2015 (2004).

Koppel T., Haldre H. Ground electrostatic field indicating subsurface water measurements in Geghard monastery, Armenia. In: Proceedings of "Earth's fields" conference; 2018

Kraus K., Droll K. INVESTIGATIONS OF SOLUBLE SALT CONTENTS IN MODERN HYDRAULIC LIME MORTARS - TEST METHOD AND FIRST RESULTS. In: International RILEM Workshop on Repair Mortars for Historic Masonry. 2005

Lacheha, A., Mertah O., Kherbeche A., & Hassoune H. Utilization of phosphogypsum in CO2 mineral sequestration by producing potassium sulphate and calcium carbonate. In: Materials Science for Energy Technologies. KeAi Chinese roots global impact; 2020

Liu G.-L., Kazarian S. G. Recent advances and applications to cultural using ATR-FTIR spectroscopy and ATR-FTIR spectroscopic imaging. In: Royal society of chemistry. 2022

Muradov M., Kot P., Markiewicz J., Lapinski S., Tobiasz A., Onisk K., Shaw A., Hashim K., Zawieska D., Mohi-Ud-Din G. Non-destructive system for in-wall moisture assessment of cultural. In: Measurements. Elsevier; 2022

Normative CNR-ICR NorMal 14/83 – Sezioni Sottili e Lucide di Materiali Lapidei: tecnica di Allestimento

Parc R. L., Champagnon B., Dianoux J., Jarry P., Martinez V. Anorthite and CaAl2Si2O8 glass: low frequency Raman spectroscopy and neutron scattering. In: Non-Crystalline Solids. 2003

Pawlyta M., Rouzaud J.-N., Duber S. Raman microspectroscopy characterization of carbon blacks: Spectral analysis and structural information. In: Carbon. 2014

Polle A., Chen S. On the salty side of life: molecular, physiological and anatomical adaptation and acclimation of trees to extreme habitats. In: Plant Cell and Environment. John Wiley & Sons Ltd; 2014

Ribeiro T., Oliveira D. V., Bracci S. The use of contact sponge method to measure water absorption in earthen heritage trated with water repellents. In: International Journal of Architectural Heritage. 2020

Ruggieri R., Davtyan S., Shaihinyan S., Ugujyan A., Orsini R., et al. Armenian karst project. In: Carbonates and Evaporites. Springer; 2022

Sahinian A. Il complesso monastico di G(h)eghard. In: Documenti di Architettura Armena | G(h)eghard. Edizioni Ares; 1973

Santo A. P., Benedetto F. D., Garzonio C. A., Pecchioni E., Salvatici T., Coppola M. Stone Architectural Decoration in Burji Era: The Northern Mausoleum in the Khanqah of Al-Nasir Faraj Ibn Barquq (Cairo). Contribution to the Knowledge and Conservation Assessment. In: heritage. MDPI; 2021

Sassoni E., Franzoni E. Influence of porosity on artificial deterioration of marble and limestone by heating. In: Applied Physics A. 2013

Sekine T., Kobayashi T., Nishio M., Takahashi E. Shock equation of state of basalt. In: Earth Planets Space. 2008

Senila M., Neag E., Cadar O., Hoaghia M.-A., Roman M., Moldovan A., Hosu A., Lupas A., Kovacs E. D. Characteristics of Volcanic Tuff from Macicasu (Romania) and Its Capacity to Remove Ammonia from Contaminated Air. In: *molecules*. Advanced Analytical Techniques in Environmental Chemistry; 2022

Siegesmund S., Gross C. J., Oriolo S., Lorsabyan T. THE ARMENIAN GEOLOGICAL RECORD Drifting Continents, Earthquakes, Volcanism, Landscapes and Geological Resources. In: Armenien. Kultur Natur Menschen. Mitteldeutscher Verlag; 2022

Siegesmund S., Pötzl C. BUILDING STONES OF ARMENIA Conservation and restoration measures as resource protection. In: Armenien. Kultur Natur Menschen. Mitteldeutscher Verlag; 2022

Stanchits S., Vinciguerra S., Dresen G., Ultrasonic Velocities, Acoustic Emission Characteristics and Crack Damage of Basalt and Granite. In: Pure and Applied Geophysics. 2006

Tornari, V. Interferometric Quantification of the Impact of Relative. In: heritage. MDPI; 2023

UNI Normal 11432-2011, Beni culturali, Materiali lapidei naturali ed artificiali - Misura della capacità di assorbimento di acqua mediante spugna di contatto

UNI Normal 13/83 – Dosaggio dei Sali Solubili

Vahramian H. Breve cronologia storica. In: Documenti di Architettura Armena | G(h)eghard. Edizioni Ares; 1973

Valluzzi M. R. On the vulnerability of historical masonry structures: analysis and mitigation. In: Materials and Structures. RILEM; 2006

Vary A. Ultrasonic measurement of material properties. In: Ultrasonic Characterization of Material Properties. NTRS; 1980.

Veneranda M., Irazola M., Pitarch A., Olivares M., Iturregui A., Castro K., Madariaga J. M. In-situ and laboratory Raman analysis in the field of cultural heritage: the case of a mural painting. In: Raman Spectroscopy. Wiley & Sons, Ltd.; 2014

Wedekind W., Harutyunyan E., Novaković N., Siegesmund S. Experimental Conservation and first Investigations on the Weathering of Geghard Monastery (Armenia). In: Monument Future: Decay and Conservation of Stone – Proceedings of the 14th International Congress on the Deterioration and Conservation of Stone. Mitteldeutscher Verlag; 2020

Widodo C. S., Sela H., Santosa D. R. The effect of NaCl concentration on the ionic NaCl solutions electrical impedance value using electrochemical impedance spectroscopy methods. In: THE 8TH ANNUAL BASIC SCIENCE INTERNATIONAL CONFERENCE: Coverage of Basic Sciences toward the World's Sustainability Challenges. 2018

Xie T., Osinski G. R., Shieh S. R. Raman study of shock effects in lunar anorthite from the Apollo missions. In: Meteoritics & Planetary Science. MET; 2021

Yilmaz S., Özkan O. T., Günay V. Crystallization kinetics of basalt glass. In: Ceramics International. 1996

Comprehensive sitography

biblio.toscana.it Pietra d'Istria, Biblio Toscana (accessed in September 2023). Available at: https://biblio.toscana.it/argomento/Pietra%20d'Istria

greenspec.co.uk The importance of breathability in old buildings, greenspec (accessed in September 2023). Available at: https://www.greenspec.co.uk/building-design/importance-of-breathability-in-old-buildings/

icomos.org ICOMOS charter Principles for the analysis, conservation and Structural Restoration of Architectural Heritage, ICOMOS international council on monuments and sites. 2003 (accessed on: September 2023). Available at: https://www.icomos.org/en/about-the-centre/179-articles-en-francais/ressources/charters-and-standards/165-icomos-charter-principles-for-the-analysis-conservation-and-structural-restoration-of-architectural-heritage

irug.org IRUG Infrared & Raman Users Group. 1993 (accessed on: September 2023). Available at: http://www.irug.org/

rruff.info RRUFF (accessed on: September 2023). Available at: https://rruff.info/

spectrabase.com SpectraBase, Wiley & Sons (accessed on: September 2023). Available at: https://spectrabase.com/

webbook.nist.gov NIST Chemistry WebBook, NIST National Institute of Standards and Technology U.S. Department of commerce (accessed on: September 2023). Available at: https://webbook.nist.gov/chemistry/name-ser/